at the wrist and the increase in the CMAP), and the distance (the length between the recording electrode and the stimulator at the wrist). We used the amplitude of the CMAP and distal velocity (distal latency divided by the distance) for further analysis. For the motor nerve conduction study, we used an EMG/evoked potential measuring system (Neuropack μ, MEB-9100, Nihon Koden, Tokyo, Japan). We used SPSS (ver. 12.0, SPSS Inc., Chicago, IL) for the statistical analysis.

PET using ^{18}F-FDG

For the ^{18}F-FDG-PET scan, we injected ~185 MBq of ^{18}F-FDG produced at the National Cardiovascular Center Research Institute using a conventional method described previously (Hamacher et al., 1986) and scanned the whole body for 48 min starting at 60 min after the injection. For the PET scan, we used a PET scanner (PCT-2000A, Toshiba Medical Systems Corp, Tokyo, Japan) that provided 47 slices in an axial field of view of 162 mm with an intrinsic resolution of 6.2 mm (trans-axial) and 6.0 mm (axial) in full-width-at-half-maximum. The scan was performed in a three-dimensional mode after the transmission scan using three rotating ^{68}Ga–^{68}Ge rod sources. The images were reconstructed in a matrix of $128 \times 128 \times 223$ (x, y, z) with a voxel size of $5.15 \times 5.15 \times 5.15$ mm (x, y, z) using a filtered back projection algorithm. The reconstructed ^{18}F-FDG radioactivity image (in Bq/ml) was scaled by the injected dose of ^{18}F-FDG per body weight of animal (Bq/g) to calculate images of SUV. The region was considered to be abnormal when the SUV value was greater than 2.5 (Al-Sugair and Coleman, 1998), and when located in the area outside of organs known to have physiologic accumulation of FDG (brain, heart, urinary tracts, and kidneys). SUV images were inspected by coronal, axial, and sagittal sections and also by the maximum intensity projection.

Immunohistochemical analysis of transplanted grafts

One year after transplantation, animals were sacrificed by an overdose of pentobarbital and perfused transcardially with 4% paraformaldehyde in 0.01 M PBS. The transplanted median nerve, including the proximal site, graft, and distal site, was dissected out and incubated in the same fixative for 6 h at 4 °C. Tissues were washed with 0.1 M PBS overnight at 4 °C, immersed in 10%, 20%, and 30% sucrose–PBS for 3 h each at 4 °C, embedded in OCT, and cut into 10-μm-thick frozen sections using a cryostat. Immunohistochemistry was performed as described elsewhere (Kitada et al., 2001). Primary antibodies used for immunohistochemistry were: anti-neurofilament (NF) rabbit polyclonal antibody (Sigma), anti-myelin-associated glycoprotein (MAG) mouse monoclonal antibody (1:100, Boehringer Ingelheim, Ingelheim am Rhein, Germany), anti-Ki67 rabbit monoclonal SP-6 IgG (1:300), and anti-CD163 mouse monoclonal IgG (1:20, Hycult Biotechnology, Uden, Netherlands). Secondary antibodies were: anti-rabbit IgG conjugated to Alexa488 (Molecular Probes) and anti-rabbit or anti-mouse IgG conjugated to Alexa568 (Molecular Probes). To assess the extent of regeneration, the ratio of the NF-positive area inside the grafted tube at the middle of the graft was calculated in three 10-μm-thick transverse sections from each animal. Statistical analysis of the ratio of NF-positive area to the total nerve area was compared using ANOVA with pairwise comparison using t-tests. To analyze the distribution of proliferating cells inside the grafted tube, immunostaining against Ki67 was done under the antigen retrieval technique using microwave (Kitada and Rowitch, 2006).

Results

Schwann cell induction from cynomolgus monkey MSCs

Cultured naïve MSCs of cynomolgus monkey are shown in Fig. 1A. When naïve MSCs were treated with BME followed by RA administration, and a set of cytokines (bFGF, FSK, PDGF, and neuregulin), their morphology changed similar to human and rat M-Schwann cells (Figs. 1B–D), suggesting the possibility of Schwann cell induction from monkey MSCs. Cells exhibiting morphological changes were evaluated to determine whether they had acquired Schwann cell phenotypes. In immunocytochemistry, Schwann cell markers including p75, GFAP, P0, and O4 became positive in monkey M-Schwann cells, while naïve MSCs or M-Schwann cells without primary antibody incubation (data not shown) showed no immunoreactivity against

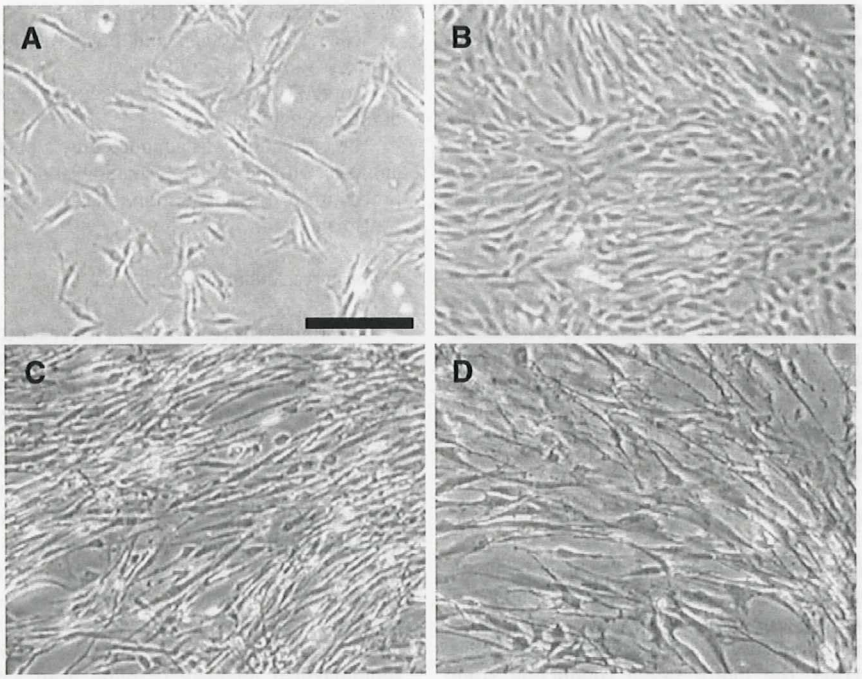

Fig. 1. Phase contrast microscopy. A: Naïve monkey MSCs, B: monkey M-Schwann cells, C: human M-Schwann cells, and D: rat M-Schwann cells. Morphological changes were evident from A to B. M-Schwann cells derived from human and rat exhibited similar morphology to those from monkey. Scale bar: 30 μm.

Please cite this article as: Wakao, S., et al., Long-term observation of auto-cell transplantation in non-human primate reveals safety and efficiency of bone marrow stromal cell-derived Schwann..., Exp. Neurol. (2010), doi:10.1016/j.expneurol.2010.01.022

these Schwann cells markers (Fig. 2). Schwann cell markers analyzed were all positive in the YST-1 cells. The rate of p75-positive cells in M-Schwann cells was estimated to be 99.0 ± 0.01% (mean ± SD). RT-PCR showed the mRNA expression of GFAP and Krox20 was weakly detected in naïve MSCs, but was up-regulated following M-Schwann cell induction. Myelin basic protein (MBP), another marker for Schwann cells, was undetectable in naïve MSCs but became clearly detectable in M-Schwann cells (Fig. 3). These results suggested that M-Schwann cells expressed markers and factors related to Schwann cell properties. We tried to determine whether M-Schwann cells sustained their expression of MSC markers such as CD90 and SMA (Supplementary Fig. 1). Whereas CD90 was not expressed in M-Schwann cells, SMA expression was recognized and the expression level of SMA was varied in each M-Schwann cell. These findings suggest that M-Schwann cells might partially trail some of the MSC characteristics at least in culture, although it is unknown whether M-Schwann cells lose or retain the MSC property during maturation in the transplanted environment.

Prior to transplantation, we constructed the graft tube made with lactic acid and E-caprolactone and filled the inside of the graft tube with collagen sponge and M-Schwann cells (see Materials and methods). Cell number was calculated to mimic endogenous Schwann cell number in an intact monkey peripheral nerve. To observe the distribution of the cells inside the graft, the graft was longitudinally cut and the nuclei of the cells were counterstained with Hoechst 33342 (Supplementary Fig. 2). Nuclei of the cells were homogenously distributed inside the graft.

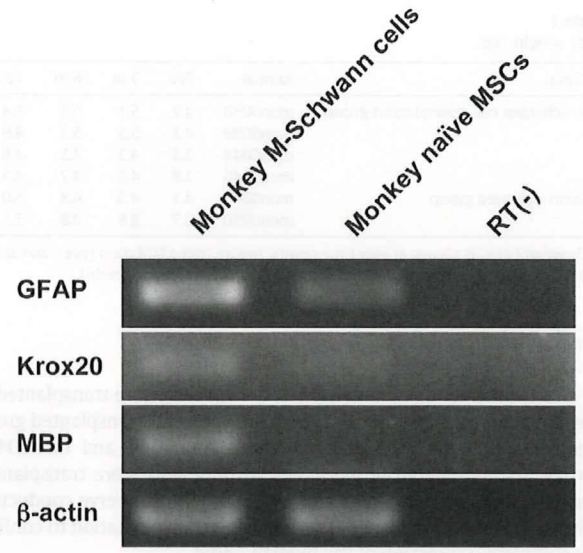

Fig. 3. RT-PCR of Schwann cell markers. Naïve MSCs slightly expressed for mRNA of GFAP and Krox20, but did not express that of myelin basic protein (MBP). Monkey M-Schwann cells, however, presented up-regulation of GFAP and Krox20 mRNA, and became clearly positive for MBP.

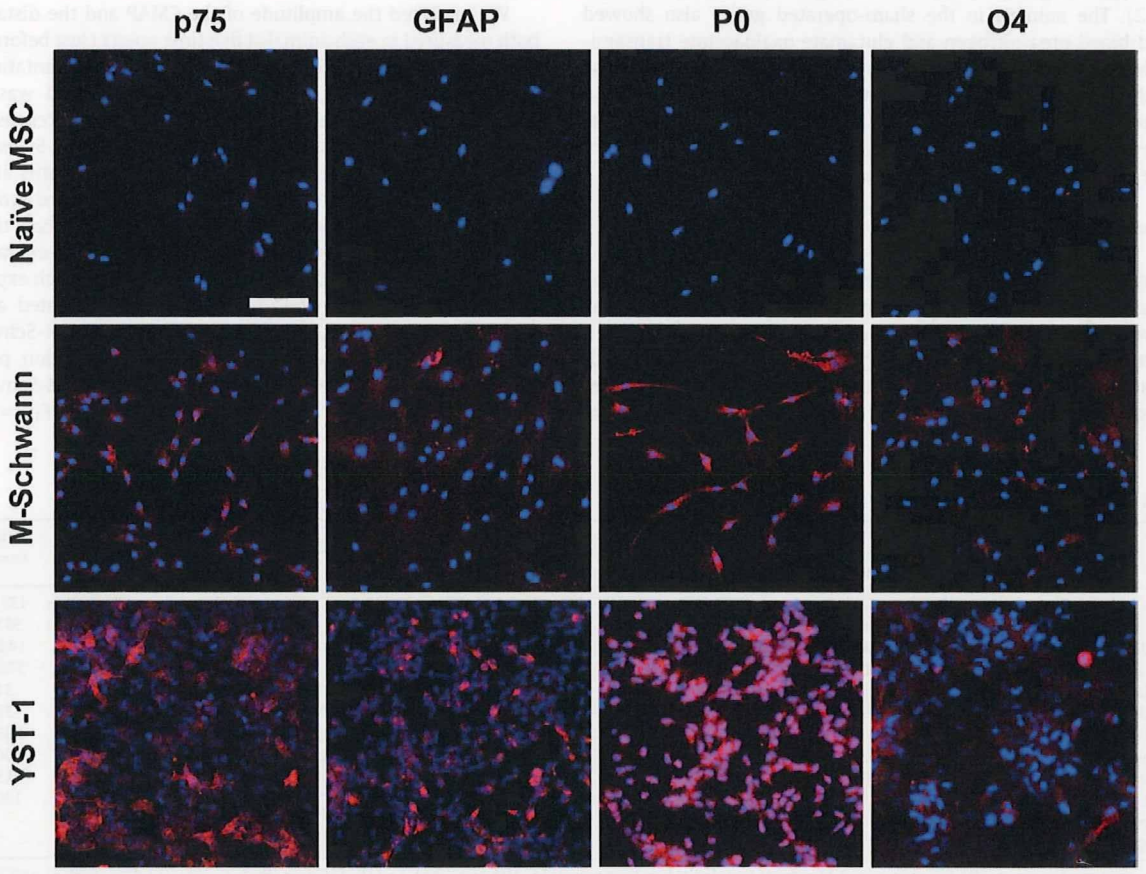

Fig. 2. Immunocytochemistry of naïve MSCs and M-Schwann cells. Initially naïve MSCs exhibited almost no immunoreactivity for Schwann cell markers (red) such as p75, GFAP, P0, and O4. After induction of Schwann cells, M-Schwann cells were positive for all Schwann cell markers: p75, GFAP, P0, and O4. YST-1 was used as a positive control and was also positive for all Schwann cells markers analyzed. DAPI (blue) was used for the counterstaining of nuclei. Scale bar: 50 μm.

Please cite this article as: Wakao, S., et al., Long-term observation of auto-cell transplantation in non-human primate reveals safety and efficiency of bone marrow stromal cell-derived Schwann..., Exp. Neurol. (2010), doi:10.1016/j.expneurol.2010.01.022

Table 1
Body weight (kg).

Group	Animal	Pre	3 m	6 m	12 m
M-Schwann cell-transplanted group	mon0038	4.2	5.1	5.5	5.4
	mon0039	4.8	5.3	5.3	4.9
	mon0044	3.8	4.3	4.5	4.9
	mon0046	3.8	4.3	4.7	4.5
Sham-operated group	mon0045	4.1	4.5	4.8	5.0
	mon0050	3.7	2.8	2.8	3.7

Body weight (kg) is shown at four time points: before transplantation (pre), and at 3, 6, and 12 months after transplantation (3 m, 6 m, and 12 m, respectively).

General health follow-up

Grafts filled with autologous M-Schwann cells were transplanted to the unilateral median nerve in the M-Schwann cell-transplanted group (monkey numbers: mon0038, mon0039, mon0044, and mon0046). For the sham-operated group, tubes without cells were transplanted (monkey numbers: mon0045 and mon0050). Motor nerve conduction velocity was measured just before and after transplantation to confirm the complete transection of the median nerve.

For follow-up of general health, body weight check and blood tests were performed at 1 to 6 month intervals after transplantation. In both the M-Schwann cell-transplanted and sham-operated groups, no considerable weight loss was observed, except in one animal in the sham-operated group (mon0050; Table 1). Creatinine, creatine kinase, glutamate oxaloacetate transaminase, glutamate pyruvate transaminase, lactate dehydrogenase, platelet, hemoglobin, red blood cell, and white blood cell levels were within normal range in the M-Schwann cell-transplanted group. Blood urea nitrogen was slightly elevated (Table 2). The animals in the sham-operated group also showed elevated blood urea nitrogen and glutamate oxaloacetate transaminase, glutamate pyruvate transaminase, and lactate dehydrogenase higher than normal values. Although the normal values of D-dimer and fibrinogen A are not established in the intact cynomolgus monkeys, the values were almost within the normal range of humans and did not increase during the follow-up period in either group.

Behavioral analysis

To assess functional recovery, general behavior, hand motion, and movement of muscles along the distribution of the affected median nerve were video-recorded and evaluated to be in 5 levels (see Materials and methods). The functional recovery score of the M-Schwann cell-transplanted group was high at 3 months while that of the sham-operated group was markedly lower even at 1 year. In the sham-operated group, because the use frequency was very low, and hand motion or food grabbing were poor due to the rigidity of the operated hand, their scores remained around 1 and 2. The M-Schwann cell-transplanted group had a mean functional recovery score of approximately 3 and 4 at 6 months. At 9 and 12 months, some monkeys in the M-Schwann cell-transplanted group achieved the highest possible score of 5 (Table 3). Actual hand movements used in feeding are shown in the video-recorded data (see movies in Supplementary information).

Table 3
Scores for hand motion recovery.

Group	Animal	3 m	6 m	9 m	12 m
M-Schwann cell-transplanted group	mon0038	3	4	5	5
	mon0039	3	4	5	5
	mon0044	4	4	5	5
	mon0046	4	A	4	4
Sham-operated group	mon0045	1	1	2	2
	mon0050	A	A	1	1

Scores for hand motion recovery at 3, 6, 9, and 12 months after surgery. In the sham-operated group, score 2 was the highest score achieved at 1 year, whereas the M-Schwann cell-transplanted group showed good recovery up to score 5.

Any animals both in the sham-operated and M-Schwann cell-transplanted groups did not exhibit self-mutilation or overgrooming in the radial palm of the hand, the innervation area of sensory branch of the transected median nerve, suggesting no abnormal sensation including dysethesia or hyperalgesia was evoked by transplanted tube and M-Schwann cells.

Motor nerve conduction study

We analyzed the amplitude of the CMAP and the distal velocity, both measured in each animal at five time points (just before and after transplantation, and 3, 6, and 12 months after transplantation; Fig. 4). The group comparison at each observation period was done by the two sample sign test, showing significant differences at 6 and 12 months after transplantation between the M-Schwann cell-transplanted and sham-operated groups. At 12 months after transplantation, the CMAP in M-Schwann cell-transplanted group nerves recovered to ~60% (mean ± SD = 7.27 ± 4.41 mV) than that of the pre-transplanted nerves (12.2 ± 0.73 mV). The sham-operated CMAP reached ~20% (2.45 ± 0.51 mV). The whole data of each experimental group was further analyzed by the two-way repeated analysis of variance (repeated ANOVA) with factors of group (M-Schwann cell-transplanted vs. sham-operated) and the observation period and found a significant effect of group in CMAP. The M-Schwann cell-transplanted group had a significantly greater CMAP ($F_{1,4} = 5.02$, one-

Table 2
Results of the blood analysis.

	M-Schwann cell-transplanted group ($n=4$)				Sham-operated group ($n=2$)				Normal values ($n=27$)
	Post-1	Post-2	Post-3	Post-4	Post-1	Post-2	Post-3	Post-4	
WBC ($\times 10^2$/μl)	116 (19)	123 (27)	107 (17)	88 (14)	122 (17)	111 (1)	117 (6)	77 (53)	133 (57)
RBC ($\times 10^4$/μl)	554 (50)	567 (59)	565 (51)	576 (56)	562 (10)	580 (5)	497.5 (67)	540 (18)	587(77)
Hb (g/dL)	13.1 (0.5)	13.5 (0.8)	13.25 (0.5)	13.7 (1.5)	13.0 (0.3)	13.5 (0.4)	12.9 (0.8)*	12.6 (0.1)	14.6(1.1)
PLT ($\times 10^4$/μl)	35.4 (14.0)	32.5 (10.0)	30.2 (7)	32.5 (11)	38.0 (3.6)	31.0 (0.1)	31.5 (0.5)	30.2 (5.0)	37.9(10.8)
GOT (IU/L)	29 (5)	28 (3)	29 (4)	36 (6)	32 (2)	46 (9)*	38 (5)	25 (1)	31(8)
GPT (IU/L)	15 (1)	26 (3)	27 (5)	34 (7)	31 (21)	64 (33)*	64 (7)**	30 (5)	36(12)
LDH (IU/L)	437 (182)	337 (30)	377 (25)	479 (116)	343 (80)	511 (123)	401 (62)	265 (35)	592(116)
CRE (mg/dL)	0.7 (0.1)	0.7 (0.1)	0.7 (01)	0.7 (0.1)	0.6 (0.0)	0.7 (0.0)	0.7 (0.1)	0.7 (0.1)	0.66(0.12)
BUN (mg/dL)	23.9 (3.5)	28.1 (4.3)**	25.6 (4.2)*	19.8 (6.1)*	27 (1.0)	30.2 (7.8)*	25.1 (2.4)	19.1 (5.7)	20.5(3.7)
CK (U/L)	147 (66)	128 (32)	69 (23)	214 (93)**	158 (44)	303 (86)**	229 (200)*	553 (4)**	126(50)
D-dimer (μg/ml)	0.7 (0.1)	1.2 (0.3)	0.9 (0.3)	–	1.3 (0.5)	1.3 (0.2)	1.1 (0.1)	–	–
Fibrinogen A (mg/dl)	–	170 (23)	190 (20)	–	–	176 (1.4)	205 (13)	–	–

Values are presented as mean (SD). For each animal, blood was sampled at four time points: 55–104 days (Post-1), 110–180 days (Post-2), 196–217 days (Post-3), and 350–470 days (Post-4) after transplantation. Normal values were obtained from animals 3 years old or younger. –: not obtained. *one or **two animals in the corresponding group had values outside the normal range of values ± 2SD. Although normal D-dimer and fibrinogen A values were not obtained in cynomolgus monkeys, they were close to the normal range of humans (D-dimer: <1.0 mg/ml and fibrinogen A <380 mg/dl).

Please cite this article as: Wakao, S., et al., Long-term observation of auto-cell transplantation in non-human primate reveals safety and efficiency of bone marrow stromal cell-derived Schwann..., Exp. Neurol. (2010), doi:10.1016/j.expneurol.2010.01.022

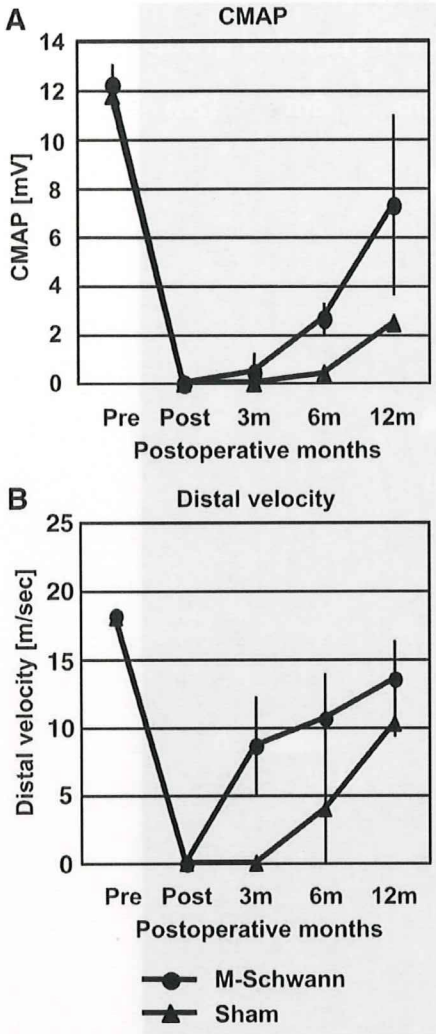

Fig. 4. Results of motor nerve conduction studies. (A) Compound muscle action potential (CMAP, in mV) of the medial nerve, (B) distal velocity (m/s) of the median nerve and (C) the actual wave forms of the CMAP for an example of the M-Schwann cell-transplanted group. Pre; before transplantation, Post; just after transplantation, 3 m, 6 m, and 12 m indicate 3, 6, and 12 months after transplantation, respectively. Values in (A, B) are presented as mean ± SD (mV and m/s, respectively).

tailed $P = 0.04$) than the sham-operated group. These findings suggest that auto-cell transplantation of M-Schwann cells significantly promoted regeneration of the median nerve motor axons distal to the transected site and that this graft contributed about 40% of the grab function at 1 year post-transplantation. In terms of distal velocity, significant promotion was observed at 3 months after transplantation by the two sample sign test, and a significant group effect ($F_{1,4} = 5.85$, one-tailed $P = 0.036$) was demonstrated by the two-way repeated ANOVA, in the M-Schwann cell-transplanted group, but the velocities at 12 months after transplantation were well recovered in both the M-Schwann cell-transplanted group (13.5 ± 4.03 m/s) and the sham-operated group (10.2 ± 1.33 m/s) to a level 60% to 75% of the pre-transplantation (18.0 ± 0.57 m/s) velocity. These findings suggest that saltatory conduction was a little accelerated by the transplanted M-Schwann cells but reached almost a similar level observed in the sham-operated group at 12 months after transplantation because of the contribution of the host Schwann cells in myelin formation and saltatory conduction.

^{18}F-FDG-PET

Although the ^{18}F-FDG-PET test is not completely specific for neoplastic cells, it sensitively detects such cells in most organs. In addition, previous studies revealed that neoplastic transformation of host Schwann cells can be detected by FDG-PET scans (Hamada et al., 2006). Thus, for each animal, we performed ^{18}F-FDG-PET scans to screen for neoplastic transformation of the grafts at 3, 6, and 12 months after transplantation.

We found no abnormal radioactivity accumulation based on standardized uptake value (SUV) images of FDG-PET at any of the three time points (Fig. 5) except in regions of physiologic accumulation and in the vein where the FDG was injected. Importantly, no apparent accumulation was observed at the transplanted site of the animals in any PET scan.

Histological analysis of the graft after 1 year

To estimate the safety of M-Schwann cell transplantation, labeling of cells prior to the transplantation such as lentivirus- or retrovirus-mediated gene introduction of green fluorescent protein or labeling with fluorescent dye was not performed. Therefore, the true ratio of Schwann cell marker expression in transplanted M-Schwann cells could not be evaluated. Furthermore, since host Schwann cells migrate from both proximal and distal nerve segments, host Schwann cells and M-Schwann cells might have intermingled within the grafted tube. For these reasons, we did not attempt to show the grafted cells inside the tube but instead examined the effect of transplanted cells. The effect of Schwann cells in the injured PNS is to promote axonal regeneration and to construct the myelin sheath for saltatory conduction (Fawcett and Keynes, 1990; Hall, 2001; Radtke and Vogt, 2009; Torigoe et al., 1996). Electrophysiological data suggested that transplanted M-Schwann cells contributed to the promotion of axonal regeneration and that myelination level was not significantly different between the M-Schwann cell-transplanted and sham-operated groups. In this regard, we evaluated the effect of transplanted cells by immunohistochemistry for NF to detect the amount of regenerated axons inside the grafted tube (McKay Hart et al., 2002). The immunohistochemistry for NF in the transverse sections of the middle portion of the grafted tube is shown in Fig. 6. Also, the NF-positive axons inside the tube seemed more condensed, particularly at the site just beneath the inner wall of the tube, in the M-Schwann cell-transplanted group compared to the control group (Figs. 6C and D). The ratios of the NF-positive area to the total nerve area in each animal were calculated (see Materials and methods) as 51.5 ± 7.55% and 33.3 ± 1.11% in the M-Schwann cell-transplanted and sham-operated groups, respectively. The ratio of the NF-positive area in the M-Schwann cell-transplanted group was significantly greater than that in the sham-operated group (one-tailed $P<0.05$, Student's t-test with Bonferroni correction). The NF-positive area

Please cite this article as: Wakao, S., et al., Long-term observation of auto-cell transplantation in non-human primate reveals safety and efficiency of bone marrow stromal cell-derived Schwann..., Exp. Neurol. (2010), doi:10.1016/j.expneurol.2010.01.022

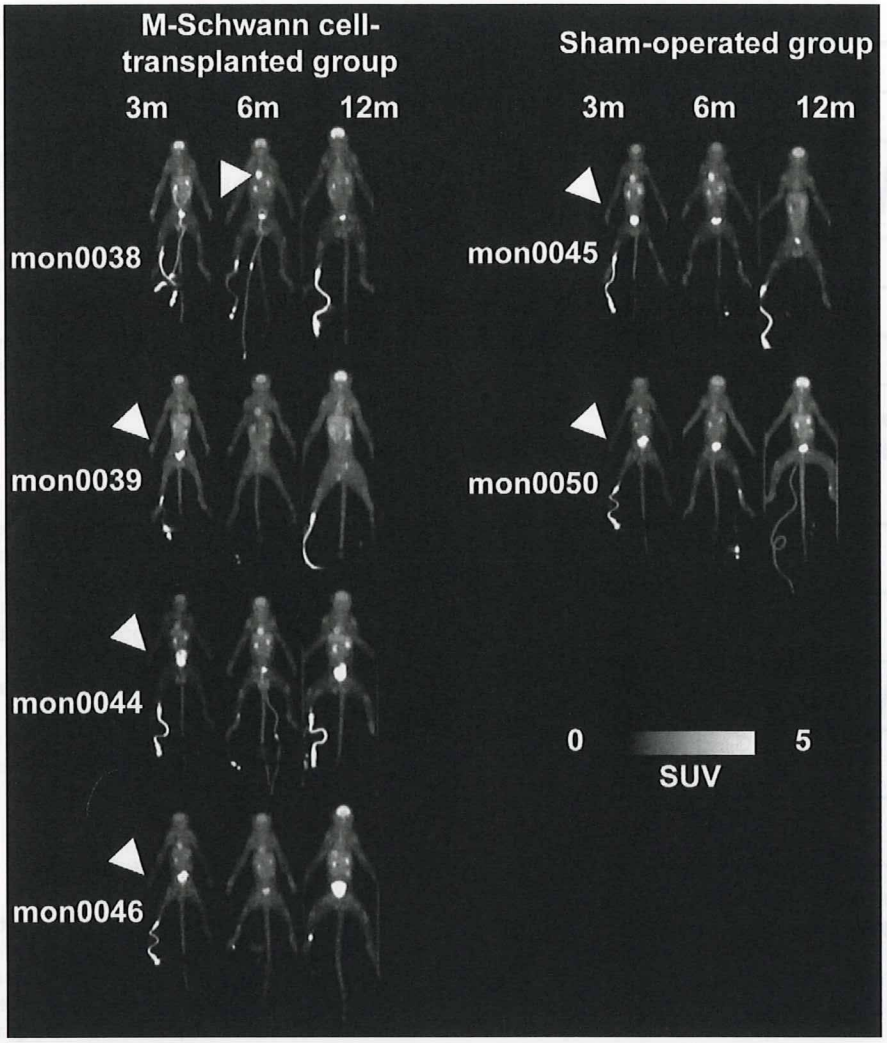

Fig. 5. Results of the whole-body ^{18}F-fluorodeoxyglucose (FDG)-positron emission tomography (PET) performed to screen for neoplastic transformation of the grafted cells. In PET images, the frontal view of the animal is presented by maximal intensity projection. Arrowheads indicate the grafted sites, the distal median nerve (left in mon0038, and right in the other animals). Abnormal accumulation (cut-off = 2.5 in SUV) was not observed in any PET scan except in regions known to have physiologic accumulations of FDG: brain, heart, kidney, urinary tracts, and injection site. SUV: standardized uptake value. 3 m, 6 m, and 12 m indicate 3, 6, and 12 months after graft transplantation.

significantly correlated with the CMAP measurement just before autopsy (measured at 12 months after operation; Pearson's correlation coefficient = 0.81, $P<0.05$). While transplanted M-Schwann cells were not distinguishable from host Schwann cells, double-immunostaining for NF and MAG on transverse sections both of the M-Schwann cell-transplanted and sham-operated groups (Figs. 6E and F, respectively) confirmed myelination of regenerated axons. As was predicted by results of electrophysiology taken at 12 months, the extent of myelination was almost similar in both experimental groups. These data suggest that the improvement observed in behavioral and electrophysiological assessment was provided by transplanted M-Schwann cells in regard to their function in promoting axonal regeneration rather than in facilitation of myelination of regenerated axons.

To observe the immune response against the transplanted graft, immunohistochemistry against CD163, a specific marker for monocytes and macrophages, was performed (Supplementary Fig. 3). Inside the graft, CD163+ cells were scarcely observed at the middle portion of the graft and some cells were found near (<300 μm) by the wall of the graft. Although CD163+ cells were observed inside the graft, the number of CD163+ cells inside the graft in the M-Schwann cell-transplanted group was as small as 1.50 ± 0.41 cells in 0.1 mm^2 and was not significantly different from 1.44 ± 0.51 cells, that in the sham-operated group, indicating that the sustained rejection of transplanted M-Schwann cells was not prominently exerted after transplantation. More CD163+ cells were observed in the wall of the graft both in the sham-operated and M-Schwann cell-transplanted groups, indicating the process of bio-degradation of the grafted tube.

Local tumor formation was evaluated by the detection of proliferating cells with Ki67-immunostaining (Fig. 7), showing no statistically significant difference between Ki67-positive cells inside the grafted tube in the M-Schwann cell-transplanted and sham-operated groups: 2.88 ± 0.67 cells and 3.25 ± 1.00 cells/0.1 mm^2, respectively. Also, these proliferating cells exhibited no mass formation. These findings indicate that transplanted M-Schwann cells did not exhibit local tumor formation.

Discussion

In the present study, we estimated the safety and effectiveness of transplanting M-Schwann cells into non-human primates over a 1-year period. Schwann cells induce neural regeneration and enable

Please cite this article as: Wakao, S., et al., Long-term observation of auto-cell transplantation in non-human primate reveals safety and efficiency of bone marrow stromal cell-derived Schwann..., Exp. Neurol. (2010), doi:10.1016/j.expneurol.2010.01.022

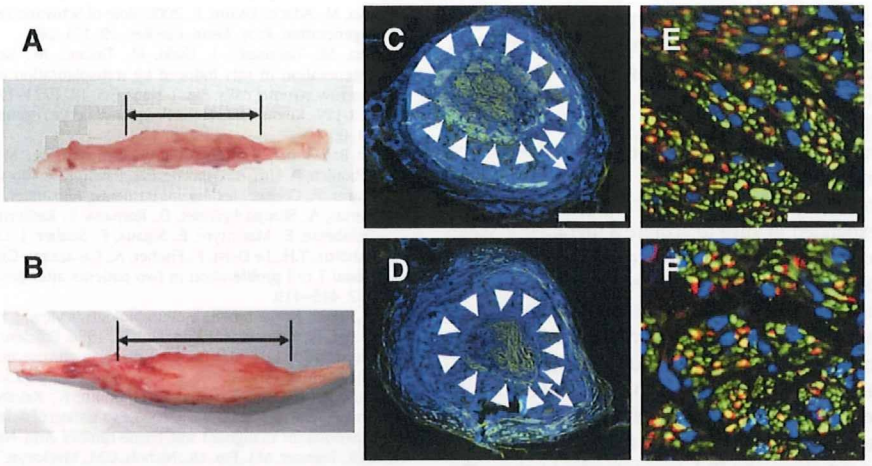

Fig. 6. Grafted monkey median nerves at 12 months. (A, B) Appearance of grafted monkey median nerves. Arrows indicate approximate position of grafts in mon0039 (M-Schwann cell-transplanted group) (A) and mon0045 (sham-operated group) (B). (C–F) Immunohistochemistry of transverse sections in the middle portion of the graft in mon0039 (M-Schwann cell-transplanted group) (C, E) and mon0045 (sham-operated group) (D, F). Immunostaining for neurofilament (NF) (green) exhibited massive axonal regeneration just beneath the inner wall of the tube (arrowheads) in the M-Schwann cell-transplanted group (C), but not in the sham-operated group (D). Arrows in C and D indicate the wall of the grafted tube. Immunofluorescence against NF (green) and myelin-associated glycoprotein (red) showed myelination of regenerated axons (E, F). The extent of myelination of regenerated axons was almost similar in both experimental groups. DAPI (blue) was used for the counterstaining of nuclei. Scale bars: 500 μm (C, D) and 40 μm (E, F).

saltatory conduction by producing myelin, and are expected to be applied to PNS and CNS injuries. In the case of the monkey study, PNS injury models are easily approved by the ethics committee for animal experimentation rather than spinal cord injury. We therefore examined the effectiveness and safety of our system in a monkey median nerve injury model. Cells that expressed Schwann cell markers could be efficiently induced from cynomolgus monkey MSCs, similar to rat and human MSCs (Dezawa et al., 2001, Shimizu et al., 2007). Auto-cell transplantation of M-Schwann cells in monkey median nerve injury model resulted in successful nerve regeneration and functional recovery.

Cell labeling is effective in tracing the fate of transplanted cells and this method is categorized into two techniques such as exogenous gene introduction and staining with a fluorescent dye. Gene introduction by virus infection such as lentivirus or retrovirus enables permanent cell labeling, while this method is also known to evoke a hazardous risk of carcinogenesis (Hacein-Bey-Abina et al., 2003). Fluorescence dyes such as DiI or PKH26 have been used for cell labeling for transplantation study but these dyes also have cytotoxicity and might not exhibit sufficient fluorescence intensity after prolonged period such as 1 year. For these reasons, we did not perform labeling of M-Schwann cells in this study. Based on the lack of any signs of tumor formation in FDG-PET scanning and in immunohistochemistry for proliferation marker for up to 1 year in any of the M-Schwann cell-transplanted animals, and the absence of serious problems in the general health and histological study, our system is very likely to be safe. In our previous report, M-Schwann cells induced from human MSCs were transplanted into a rat model of sciatic nerve transection under immunosuppression, and were shown to contribute to re-myelination of regenerating axons and functional recovery (Shimizu et al., 2007). Also, we previously examined the safety of M-Schwann cells induced from human MSCs transplanted into uninjured nude-mice striatum followed-up for 6 months (unpublished data). Tumor formation was not observed in pathologic analysis and the general health of transplanted nude-mice showed no serious problems. These results together support the idea that human MSC-derived Schwann cells may also be safe and effective for cell-based therapy.

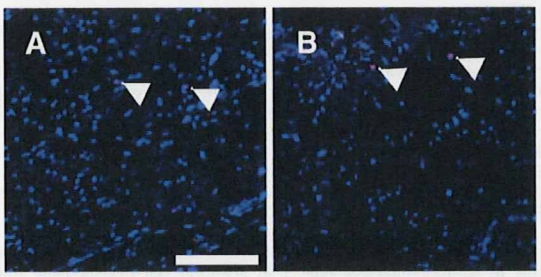

Fig. 7. Immunohistochemistry inside the grafted tube. Small numbers of Ki67-positive cells (red, arrowheads) were found in both the M-Schwann cell-transplanted (A) and also sham-operated (B) groups. DAPI (blue) was used for the counterstaining of nuclei. Scale bar: 100 μm.

Our results indicate that the M-Schwann cells contributed to functional recovery after transplantation in the injured PNS. Electrophysiology demonstrated that CMAP was much improved in the M-Schwann cell-transplanted group compared with the sham-operated group, suggesting regeneration of a larger number of axons promoted by the transplanted M-Schwann cells in this group. This concept was confirmed by histological analysis. The area positive for NF, being considered to be correlated with CMAP, was larger in the M-Schwann cell-transplanted group than in the sham-operated group.

In previous studies, we have demonstrated the myelin formation of M-Schwann cells induced from rat MSCs after transplantation into the injured PNS models even in the ultrastructural level (Dezawa et al., 2001; Ishikawa et al., 2009). In this study, electrophysiological data regarding distal velocity was accelerated in the M-Schwann cell-transplanted group compared with those of the sham-operated group. However, the biodegradable conduit used in this study itself has the property to support regenerating axons (Hisasue et al., 2005). As mentioned in Results, host Schwann cells also join to promote axonal regeneration and to form myelin sheath. This process might be enhanced by the biodegradable conduit used in this study and might mask the function of M-Schwann cells on saltatory conduction at later observation period such as 6 and 12 months after transplantation. Whether the transplanted M-Schwann cells can form myelin sheath to contribute efficient saltatory conduction should be assessed in future studies by labeling cells with either a genetic modification or fluorescent dyes prior to transplantation.

Because the induction system for M-Schwann cells comprises a cell density adjustment at the first step followed by a series of treatments with BME, RA, and a set of cytokines, M-Schwann cells can be induced

Please cite this article as: Wakao, S., et al., Long-term observation of auto-cell transplantation in non-human primate reveals safety and efficiency of bone marrow stromal cell-derived Schwann..., Exp. Neurol. (2010), doi:10.1016/j.expneurol.2010.01.022

by a rather simple and stable process without gene introduction, and thus the system is a realistic source of cell therapy for PNS and CNS regeneration. The induction of cells with Schwann cell properties was recently reported in embryonic stem cells and skin-derived neural crest cells, but their effectiveness and safety in terms of tumor formation and problems that might arise need to be examined because of potential ethical concerns (Roth et al., 2007).

MSCs provide potential possibilities for clinical application, since they can be efficiently expanded in vitro to acquire a therapeutic scale. Different from embryonic stem cells or fetus/embryo-derived cells, MSCs are easily accessible through aspiration of the bone marrow, and can be easily expanded in large scale for auto-transplantation. MSCs can be collected without serious ethical problems, and there is no need to use fertilized eggs or fetuses, which is a great advantage for clinical use. In addition, as MSCs are also obtained from marrow banks, transplantation of induced cells with the same HLA subtype from a healthy donor may minimize the risks of rejection in allo-transplantation.

In the present study, we chose the PNS injury model to show the safety and efficiency of M-Schwann cells, in which M-Schwann cells were induced prior to, and transplanted immediately after, the injury. This model, however, is not a representative of clinical situations. Virtually, it needs more than 1 week to prepare M-Schwann cells after harvesting MSCs. Further studies are necessary for confirming the effectiveness of M-Schwann cells in delayed transplantation in PNS injury.

Our previous studies have demonstrated that Schwann cells induced from MSCs exert trophic effects, provide a strong foothold for regenerating axons, and re-construct myelin to support saltatory conduction (Dezawa et al., 2001; Ishikawa et al., 2009; Kamada et al., 2005; Mimura et al., 2004; Shimizu et al., 2007; Someya et al., 2008). Therefore, induced Schwann cells are a valuable candidate source for cell therapy in peripheral nerve injury, and this study suggests that auto-cell transplantation of M-Schwann cells is also hopeful for application to spinal cord injury.

Acknowledgments

We thank to Dr. J. J. Archelos (Karl-Franzens Universitat, Graz, Austria) for providing us the P0 antibody and to Ms. Mori E., Ms. Kotera J. and Ms. Mamiya R. for their technical assistance. This study was supported by the Program for Promotion of Fundamental Studies in Health Sciences of the National Institute of Biomedical Innovation (NIBIO, 05-6) and by the Health and Labor Sciences Research Grants of "Research on Psychiatric and Neurological Diseases and Mental Health" from the Ministry of Health, Labor and Welfare. The study was also supported by Grant-in-Aid for Scientific Research (B) (19390074) from the Ministry of Education, Culture, Sports, Science and Technology Japan.

Appendix A. Supplementary data

Supplementary data associated with this article can be found, in the online version, at doi:10.1016/j.expneurol.2010.01.022.

References

Ahmed, Z., Brown, R.A., Ljungberg, C., Wiberg, M., Terenghi, G., 1999. Nerve growth factor enhances peripheral nerve regeneration in non-human primates. Scand. J. Plast. Reconstr. Surg. Hand Surg. 33, 393–401.

Al-Sugair, A., Coleman, R.E., 1998. Applications of PET in lung cancer. Semin. Nucl. Med. 28, 303–319.

Archibald, S.J., Shefner, J., Krarup, C., Madison, R.D., 1995. Monkey median nerve repaired by nerve graft or collagen nerve guide tube. J. Neurosci. 15, 4109–4123.

Auba, C., Hontanilla, B., Arcocha, J., Gorria, O., 2006. Peripheral nerve regeneration through allografts compared with autografts in FK506-treated monkeys. J. Neurosurg. 105, 602–609.

Bunge, M.B., 2002. Bridging the transected or contused adult rat spinal cord with Schwann cell and olfactory ensheathing glia transplants. Prog. Brain Res. 137, 275–282.

Bunge, M.B., 2008. Novel combination strategies to repair the injured mammalian spinal cord. J. Spinal Cord Med. 31, 262–269.

Dezawa, M., Adachi-Usami, E., 2000. Role of Schwann cells in retinal ganglion cell axon regeneration. Prog. Retin. Eye Res. 19, 171–204.

Dezawa, M., Takahashi, I., Esaki, M., Takano, M., Sawada, H., 2001. Sciatic nerve regeneration in rats induced by transplantation of in vitro differentiated bone-marrow stromal cells. Eur. J. NeuroSci. 14, 1771–1776.

Fawcett, J.W., Keynes, R.J., 1990. Peripheral nerve regeneration. Annu. Rev. Neurosci. 13, 43–60.

Hacein-Bey-Abina, S., Von Kalle, C., Schmidt, M., McCormack, M.P., Wulffraat, N., Leboulch, P., Lim, A., Osborne, C.S., Pawliuk, R., Morillon, E., Sorensen, R., Forster, A., Fraser, P., Cohen, J.I., de Saint Basile, G., Alexander, I., Wintergerst, U., Frebourg, T., Aurias, A., Stoppa-Lyonnet, D., Romana, S., Radford-Weiss, I., Gross, F., Valensi, F., Delabesse, E., Macintyre, E., Sigaux, F., Soulier, J., Leiva, L.E., Wissler, M., Prinz, C., Rabbitts, T.H., Le Deist, F., Fischer, A., Cavazzana-Calvo, M., 2003. LMO2-associated clonal T cell proliferation in two patients after gene therapy for SCID-X1. Science 302, 415–419.

Hall, S., 2001. Nerve repair: a neurobiologist's view. J. Hand Surg. [Br] 26, 129–136.

Hamacher, K., Coenen, H.H., Stocklin, G., 1986. Efficient stereospecific synthesis of no-carrier-added 2-[18F]-fluoro-2-deoxy-D-glucose using aminopolyether supported nucleophilic substitution. J. Nucl. Med. 27, 235–238.

Hamada, K., Tomita, Y., Ueda, T., Enomoto, K., Kakunaga, S., Myoui, A., Higuchi, I., Yoshikawa, H., Hatazawa, J., 2006. Evaluation of delayed 18F-FDG PET in differential diagnosis for malignant soft-tissue tumors. Ann. Nucl. Med. 20, 671–675.

Hess, J.R., Brenner, M.J., Fox, I.K., Nichols, C.M., Myckatyn, T.M., Hunter, D.A., Rickman, S.R., Mackinnon, S.E., 2007. Use of cold-preserved allografts seeded with autologous Schwann cells in the treatment of a long-gap peripheral nerve injury. Plast. Reconstr. Surg. 119, 246–259.

Hill, C.E., Moon, L.D., Wood, P.M., Bunge, M.B., 2006. Labeled Schwann cell transplantation: cell loss, host Schwann cell replacement, and strategies to enhance survival. Glia 53, 338–343.

Hisasue, S., Kato, R., Sato, Y., Suetomi, T., Tabata, Y., Tsukamoto, T., 2005. Cavernous nerve reconstruction with a biodegradable conduit graft and collagen sponge in the rat. J. Urol. 173, 286–291.

Ishikawa, N., Suzuki, Y., Dezawa, M., Kataoka, K., Ohta, M., Cho, H., Ide, C., 2009. Peripheral nerve regeneration by transplantation of BMSC-derived Schwann cells as chitosan gel sponge scaffolds. J. Biomed. Mater. Res. A 89, 1118–1124.

Jiang, L., Zhu, J.K., Liu, X.L., Xiang, P., Hu, J., Yu, W.H., 2008. Differentiation of rat adipose tissue-derived stem cells into Schwann-like cells in vitro. NeuroReport 19, 1015–1019.

Kamada, T., Koda, M., Dezawa, M., Yoshinaga, K., Hashimoto, M., Koshizuka, S., Nishio, Y., Moriya, H., Yamazaki, M., 2005. Transplantation of bone marrow stromal cell-derived Schwann cells promotes axonal regeneration and functional recovery after complete transection of adult rat spinal cord. J. Neuropathol. Exp. Neurol. 64, 37–45.

Kingham, P.J., Kalbermatten, D.F., Mahay, D., Armstrong, S.J., Wiberg, M., Terenghi, G., 2007. Adipose-derived stem cells differentiate into a Schwann cell phenotype and promote neurite outgrowth in vitro. Exp. Neurol. 207, 267–274.

Kitada, M., Chakrabortty, S., Matsumoto, N., Taketomi, M., Ide, C., 2001. Differentiation of choroid plexus ependymal cells into astrocytes after grafting into the pre-lesioned spinal cord in mice. Glia 36, 364–374.

Kitada, M., Rowitch, D.H., 2006. Transcription factor co-expression patterns indicate heterogeneity of oligodendroglial subpopulations in adult spinal cord. Glia 54, 35–46.

Lee, S.J., Lim, A.Y., Lim, I.J., Lim, T.C., Pho, R.W., 2008. Innervation of the face studied using modifications to Sihler's technique in a primate model. Plast. Reconstr. Surg. 121, 1188–1205.

McKay Hart, A., Brannstrom, T., Wiberg, M., Terenghi, G., 2002. Primary sensory neurons and satellite cells after peripheral axotomy in the adult rat: timecourse of cell death and elimination. Exp. Brain Res. 142, 308–318.

Mimura, T., Dezawa, M., Kanno, H., Sawada, H., Yamamoto, I., 2004. Peripheral nerve regeneration by transplantation of bone marrow stromal cell-derived Schwann cells in adult rats. J. Neurosurg. 101, 806–812.

Mligiliche, N.L., Tabata, Y., Kitada, M., Endoh, K., Okamato, K., Fujimoto, E., Ide, C., 2003. Poly lactic acid–caprolactone copolymer tube with a denatured skeletal muscle segment inside as a guide for peripheral nerve regeneration: a morphological and electrophysiological evaluation of the regenerated nerves. Anat. Sci. Int. 78, 156–161.

Nagane, K., Kitada, M., Wakao, S., Dezawa, M., Tabata, Y., 2009. Practical induction system for dopamine-producing cells from bone marrow stromal cells using spermine-pullulan-mediated reverse transfection method. Tissue Eng. Part A 15, 1655–1665.

Pittenger, M.F., Mackay, A.M., Beck, S.C., Jaiswal, R.K., Douglas, R., Mosca, J.D., Moorman, M.A., Simonetti, D.W., Craig, S., Marshak, D.R., 1999. Multilineage potential of adult human mesenchymal stem cells. Science 284, 143–147.

Plant, G.W., Chirila, T.V., Harvey, A.R., 1998. Implantation of collagen IV/poly(2-hydroxyethyl methacrylate) hydrogels containing Schwann cells into the lesioned rat optic tract. Cell Transplant. 7, 381–391.

Prockop, D.J., 1997. Marrow stromal cells as stem cells for nonhematopoietic tissues. Science 276, 71–74.

Radtke, C., Vogt, P.M., 2009. Peripheral nerve regeneration: a current perspective. Eplasty 9, e47.

Roth, T.M., Ramamurthy, P., Ebisu, F., Lisak, R.P., Bealmear, B.M., Barald, K.F., 2007. A mouse embryonic stem cell model of Schwann cell differentiation for studies of the role of neurofibromatosis type 1 in Schwann cell development and tumor formation. Glia 55, 1123–1133.

Shimizu, S., Kitada, M., Ishikawa, H., Itokazu, Y., Wakao, S., Dezawa, M., 2007. Peripheral nerve regeneration by the in vitro differentiated-human bone marrow stromal cells with Schwann cell property. Biochem. Biophys. Res. Commun. 359, 915–920.

Please cite this article as: Wakao, S., et al., Long-term observation of auto-cell transplantation in non-human primate reveals safety and efficiency of bone marrow stromal cell-derived Schwann..., Exp. Neurol. (2010), doi:10.1016/j.expneurol.2010.01.022

Someya, Y., Koda, M., Dezawa, M., Kadota, T., Hashimoto, M., Kamada, T., Nishio, Y., Kadota, R., Mannoji, C., Miyashita, T., Okawa, A., Yoshinaga, K., Yamazaki, M., 2008. Reduction of cystic cavity, promotion of axonal regeneration and sparing, and functional recovery with transplanted bone marrow stromal cell-derived Schwann cells after contusion injury to the adult rat spinal cord. J. Neurosurg. Spine 9, 600–610.

Torigoe, K., Tanaka, H.F., Takahashi, A., Awaya, A., Hashimoto, K., 1996. Basic behavior of migratory Schwann cells in peripheral nerve regeneration. Exp. Neurol. 137, 301–308.

Vukovic, J., Plant, G.W., Ruitenberg, M.J., Harvey, A.R., 2007. Influence of adult Schwann cells and olfactory ensheathing glia on axontarget cell interactions in the CNS a comparative analysis using a retinotectal cograft model. Neuron Glia Biol. 3, 105–117.

Xu, Y., Liu, Z., Liu, L., Zhao, C., Xiong, F., Zhou, C., Li, Y., Shan, Y., Peng, F., Zhang, C., 2008. Neurospheres from rat adipose-derived stem cells could be induced into functional Schwann cell-like cells in vitro. BMC Neurosci. 9, 21.

Please cite this article as: Wakao, S., et al., Long-term observation of auto-cell transplantation in non-human primate reveals safety and efficiency of bone marrow stromal cell-derived Schwann..., Exp. Neurol. (2010), doi:10.1016/j.expneurol.2010.01.022

Journal of Cerebral Blood Flow & Metabolism (2010) 30, 663–673

www.jcbfm.com

Measurement of density and affinity for dopamine D_2 receptors by a single positron emission tomography scan with multiple injections of [^{11}C]raclopride

Yoko Ikoma[1,2], Hiroshi Watabe[1], Takuya Hayashi[1], Yoshinori Miyake[1], Noboru Teramoto[1], Kotaro Minato[2] and Hidehiro Iida[1]

[1]*Department of Investigative Radiology, National Cardiovascular Center Research Institute, Osaka, Japan;* [2]*Biomedical Imaging and Informatics, Graduate School of Information Science, Nara Institute of Science and Technology, Nara, Japan*

Positron emission tomography (PET) with [^{11}C]raclopride has been used to investigate the density (B_{max}) and affinity (K_d) of dopamine D_2 receptors related to several neurological and psychiatric disorders. However, in assessing the B_{max} and K_d, multiple PET scans are necessary under variable specific activities of administered [^{11}C]raclopride, resulting in a long study period and unexpected physiological variations. In this paper, we have developed a method of multiple-injection graphical analysis (MI-GA) that provides the B_{max} and K_d values from a single PET scan with three sequential injections of [^{11}C]raclopride, and we validated the proposed method by performing numerous simulations and PET studies on monkeys. In the simulations, the three-injection protocol was designed according to prior knowledge of the receptor kinetics, and the errors of B_{max} and K_d estimated by MI-GA were analyzed. Simulations showed that our method could support the calculation of B_{max} and K_d, despite a slight overestimation compared with the true magnitudes. In monkey studies, we could calculate the B_{max} and K_d of diseased or normal striatum in a 150 mins scan with the three-injection protocol of [^{11}C]raclopride. Estimated B_{max} and K_d values of D_2 receptors in normal or partially dopamine-depleted striatum were comparable to the previously reported values.

Journal of Cerebral Blood Flow & Metabolism (2010) **30,** 663–673; doi:10.1038/jcbfm.2009.239; published online 11 November 2009

Keywords: [^{11}C]raclopride; dopamine D_2 receptors; graphical analysis; multiple injections; positron emission tomography

Introduction

Positron emission tomography (PET) with [^{11}C]raclopride has been widely used to investigate the availability of striatal dopamine D_2 receptors *in vivo* (Farde *et al*, 1985; Köhler *et al*, 1985; Hall *et al*, 1988). A number of postmortem studies have shown that the abundance of dopamine D_2 receptor is elevated in striatum samples from untreated patients with Parkinson's disease (Guttman and Seeman, 1985; Seeman *et al*, 1987) and in schizophrenic patients who had never taken antipsychotics (Cross *et al*, 1981; Joyce *et al*, 1988). The PET measurements have made it possible to quantify *in vivo* the density and apparent affinity of receptors by systematically varying the specific activity (or mass) of an administered radioligand (see for example, Farde *et al*, 1986). A study of Parkinson's disease by Rinne *et al* (1995) with *in vivo* PET showed increased density and unchanged affinity of dopamine D_2 receptors in the putamen in comparison with healthy controls. In corresponding studies of schizophrenia, early findings with [^{11}C]*N*-methylspiperone indicated elevated D_2 binding, which was not replicated in some subsequent studies with [^{11}C]raclopride (Wong *et al*, 1986; Farde *et al*, 1987, 1990). Dysfunction of dopamine receptors has also been suggested in other neurodegenerative or psychiatric diseases (e.g., multiple-system atrophy, progressive supranuclear palsy, and attention-deficit hyperactivity disorders); however, there have been only a few studies that

Correspondence: Dr H Watabe, Department of Investigative Radiology, National Cardiovascular Center Research Institute, 5-7-1, Fujishirodai, Suita, Osaka 565-8565, Japan.
E-mail: watabe@ri.ncvc.go.jp
Received 11 September 2009; revised 13 October 2009; accepted 19 October 2009; published online 11 November 2009

examined receptor function directly related to density and affinity. This might be due to the inherent difficulty in measuring absolute receptor abundance based on PET recordings.

In PET scans, to determine the density and affinity of receptors directly as parameters of kinetic model, it is necessary to apply a compartmental analysis based on a two-tissue compartment five-parameter model including density of receptors B_{max} (pmol/mL), bimolecular association rate constant k_{on} (mL/pmol/min), and unimolecular dissociation rate constant k_{off} (min^{-1}) (Farde *et al*, 1989). However, since data from a single PET scan are not enough to determine the B_{max} and k_{on} individually, multiple PET scans should be taken with different molar amounts of injected ligand. In addition, model parameters are estimated by a nonlinear least squares fitting with the metabolite-corrected plasma input function, so the solutions are often unstable and sensitive to statistical noise, and invasive arterial sampling is required to use this method.

Farde *et al* (1986, 1989) determined the value of B_{max} and apparent affinity K_d ($=k_{off}/k_{on}$) by a graphical analysis using a time-activity curve (TAC) of the specifically bound target region and a reference region where specific bindings are negligible. In this method, the ratio of specific bound and free ligand concentrations at the equilibrium state are plotted versus the concentration of specific bound ligand, and B_{max} and K_d are estimated from the slope and intercept of the regression line. Other groups also used the value of distribution volume ratio − 1 estimated from the graphical analysis of Logan *et al* (1996), instead of the ratios of specific bound and free concentration, to obtain stable values of the *y*-axis quantity (Logan *et al*, 1997; Doudet and Holden, 2003; Doudet *et al*, 2003). These methods are practical, because they do not require arterial blood sampling, and their respective estimation processes are easy to carry out. However, to estimate the regression line of a graphical plot, multiple PET scans (at least two or three) are required under variable molar amounts of administered ligand, so scans have been performed on separate days. Even in quantitative PET scans, the separate day protocol may suffer from interday or intraday variations in physiologic conditions, such as cerebral blood pressure, flow, and receptor bindings, which may affect the accuracy of the estimates.

We developed a method, called the multiple-injection simplified reference tissue model (MI-SRTM), to measure the change in binding potential ($BP_{ND}=k_3/k_4$ (Mintun *et al*, 1984)) of dopamine D_2 receptors from a single session of PET scanning with multiple injections of [^{11}C]raclopride (Watabe *et al*, 2006; Ikoma *et al*, 2009), and we showed that this method could detect the change in BP_{ND} because of an increase in mass of administered [^{11}C]raclopride in a short scanning period, which is a prerequisite for measuring the saturation binding parameters as steady state. In this study, we extend our earlier report for estimating B_{max} and K_d from a single session of PET scanning with triple injections of [^{11}C]raclopride using MI-SRTM and the graphical analysis, and we validated the proposed method by performing numerous simulations and studies on monkeys using PET and [^{11}C]raclopride.

Materials and methods

Theory

Graphical Analysis with a Reference Region for Estimation of Density and Affinity: Graphical analysis based on the Scatchard plot (Scatchard, 1949) has been used to estimate the values of B_{max} and K_d from as series of PET recordings with various molar amounts of administered ligand (Farde *et al*, 1986). In brief, the ratios (B/F) of specific bound ligand concentration (B [pmol/mL]) and free ligand concentration (F [pmol/mL]) at equilibrium are plotted versus B. In this plot, the slope and *x*-intercept represent $-1/K_d$ and B_{max}, respectively. In general, for graphical analysis without arterial blood sampling, the total radioligand concentration in the reference region (C_r [Bq/mL]), where specific bindings are negligible, is used as an estimate of the free radioligand concentration in the target region (C_f [Bq/mL]), that is $C_f^{ref}=C_r$, and the specific binding radioligand concentration in the target region (C_b [Bq/mL]) is defined as radioactivity in the target region (C_t [Bq/mL]) reduced with C_r, that is $C_b^{ref}=C_t-C_r$ (Figure 1). The radioactivity concentrations of C_f^{ref} and C_b^{ref}, at the point in time when dC_b^{ref}/dt is 0 (T_{eq}), are divided by a specific activity of the administered ligand, and used as F and B at the transient equilibrium in the graphical analysis

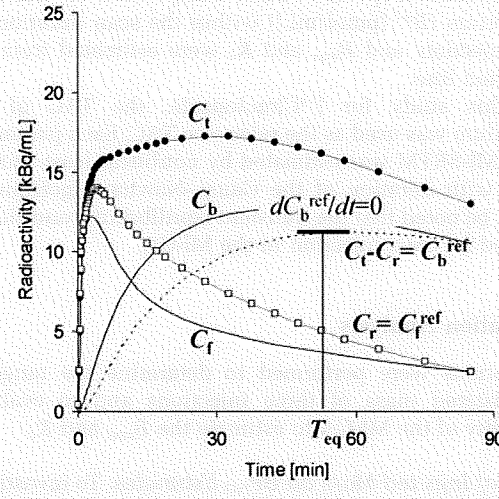

Figure 1 An example of simulated TACs for the striatum (C_t), free (C_f), and specific bound (C_b) concentrations in the striatum, the cerebellum used as a reference region (C_r) and bound concentration in the striatum estimated using a reference region ($C_b^{ref}=C_t-C_r$) with $K_1=0.033$, $K_1/k_2=0.59$, $k_{on}=0.0033$, $B_{max}=25.7$, $k_4=0.034$ for the striatum, and $K_1=0.034$, $K_1/k_2=0.36$, $k_3=0.022$, $k_4=0.034$ for the cerebellum. The time point of $dC_b^{ref}/dt=0$ (T_{eq}) is considered the transient equilibrium, and bound concentration at the equilibrium (B^{ref}) is obtained from the radioactivity concentration of C_b^{ref} at T_{eq}.

(Farde *et al*, 1989). In our study, we use the nomenclature B^{ref} and F^{ref} to represent the concentrations otherwise known as B and F. The value of the y axis, B^{ref}/F^{ref}, is sometimes replaced by the binding potential estimated by the graphical analysis of Logan *et al* (1996) or some other method (Logan *et al*, 1997; Doudet and Holden, 2003; Doudet *et al*, 2003).

Multiple-Injection Simplified Reference Tissue Model for Estimation of Binding Potential: A simplified reference tissue model (SRTM) can provide three parameters (R_1, k_2, BP_{ND}) without invasive arterial blood sampling by using a TAC of the reference region (Lammertsma and Hume, 1996). The MI-SRTM extended this SRTM for sequential multiple injections in a single session of PET scanning by taking into account the residual radioactivity in the target tissue at the time of each injection. As such, the magnitude of BP_{ND} for the ith injection is described in the following terms (Ikoma *et al*, 2009):

$$C_{ti}(t) = R_{1i}C_{ri}(t) + \left(k_{2i} - \frac{R_{1i}k_{2i}}{1+\mathrm{BP_{NDi}}}\right)e^{-\frac{k_{2i}}{1+\mathrm{BP_{NDi}}}t} \otimes C_{ri}(t) + (C_{ti}(0) - R_{1i}C_{ri}(0))e^{-\frac{k_{2i}}{1+\mathrm{BP_{NDi}}}t} \quad (1)$$

where C_{ti} and C_{ri} are the radioactivity concentrations in the target and reference region, respectively, and t is the time from the start of the ith injection.

Multiple-Injection Graphical Analysis for Estimation of Density and Affinity: The conventional graphical analysis was applied to the B_{max} and K_d estimations with the multiple-injection approach. In this multiple-injection graphical analysis (MI-GA), the BP_{ND} calculated for each injection using MI-SRTM was plotted as a function of the concentration of specific bound raclopride at the transient equilibrium (B^{ref} [pmol/mL]) within the scan duration for each injection, and B_{max} and K_d were estimated from the regression line.

In this study for [^{11}C]raclopride, the TAC of the cerebellum was used as the reference TAC. Each parameter in the MI-SRTM was estimated by nonlinear least squares fitting with iteration of the Gauss–Newton algorithm. It should be noted that the transient equilibrium condition is required for each injection in the MI-GA.

Simulation Analysis

Simulations were performed to determine the range of administered mass of three injections and to evaluate feasibility of the MI-GA to estimate the B_{max} and K_d.

Effect of Injected Mass on BP_{ND} Estimates: To investigate the effect of the administered molar amount of [^{11}C]raclopride on BP_{ND} estimates and to determine the molar amount of three injections for monkey studies, a relationship between BP_{ND} and B^{ref} was obtained by a computer simulation. Noiseless TACs of the striatum and cerebellum were generated with a measured plasma TAC and assumed parameter values derived from measurements taken from the monkey studies. The TAC of the cerebellum was simulated with a conventional two-tissue compartment four-parameter model with assumed parameter values obtained earlier in our monkey studies: $K_1 = 0.034$ (mL/mL/min) $K_1/k_2 = 0.36$, $k_3 = 0.022$ (min^{-1}), $k_4 = 0.034$ (min^{-1}). Meanwhile, the TAC of the striatum was simulated with a two-tissue compartment five-parameter model expressed as Equation (2) by solving these differential equations with the numerical analysis of fourth-order Runge–Kutta method with assumed parameter values $K_1 = 0.033$ (mL/mL/min), $K_1/k_2 = 0.59$, $k_{on} = 0.0033$ (mL/pmol/min), $B_{max} = 25.7$ (pmol/mL), $k_4 = 0.026$ (min^{-1}), and SA = 37 (GBq/μmol):

$$\begin{aligned} \frac{dC_f}{dt} &= K_1 C_p(t) - \left(k_2 + k_3'(t)\right)C_f(t) + k_4 C_b(t) \\ \frac{dC_b}{dt} &= k_3'(t)C_f(t) - k_4 C_b(t) \\ k_3'(t) &= k_{on}\left(B_{max} - \frac{C_b(t)}{SA}\right) \end{aligned} \quad (2)$$

where C_f and C_b are the concentrations of radioactivity for free and specifically bound [^{11}C]raclopride in tissue, respectively; and SA is the specific activity of administered [^{11}C]raclopride.

As reference, the relationships between B^{ref} and BP_{ND} or B^{ref}/F^{ref} were investigated in the case of a single injection of [^{11}C]raclopride by varying injected mass. TACs of the striatum and cerebellum for the single injection with a 50 mins scan were generated using the measured plasma TAC of a single injection in which the input plasma TAC was amplified, such that the corresponding mass increased from 1 to 500 nmol per injection. In each simulated TAC, BP_{ND} values were estimated by the SRTM, and then, B^{ref}/F^{ref} and B^{ref} were calculated by the transient equilibrium with the cerebellum TAC.

Next, TACs of the striatum and cerebellum for three injections at 50 mins intervals were generated using the plasma TAC of three sequential injections in which the input plasma TAC was amplified so that the mass of the first and second injections would be 1.5 and 10 nmol/kg, and the mass of the third injection would be 1.5 to 150 nmol/kg. In each simulated TAC, BP_{ND} values were estimated by the MI-SRTM, and B^{ref}/F^{ref} and B^{ref} for the third injection was calculated by the transient equilibrium with the cerebellum TAC. The relationships between B^{ref} and BP_{ND} or B^{ref}/F^{ref} for the third injection were investigated, and compared with that for the single injection.

Estimation of B_{max} and K_d Values by the Multiple-Injection Graphical Analysis: The reliability of B_{max} and K_d estimates by the graphical analysis was investigated for the proposed sequential multiple-injection approach (single PET scan) and compared with that for the conventional nonsequential approach (three PET scans on different days, such that no residual mass remained). Noiseless TACs of the striatum and cerebellum were simulated using assumed parameters of the two-tissue compartment model mentioned above and the plasma input function for three injections in which the magnitude of each 'virtual' input function was adjusted so that the injection mass would be 1.5, 10, or 30 nmol/kg determined from the simulation study mentioned above, with 50 mins intervals as reported

by Ikoma *et al* (2009). In the striatum TACs, B_{max} values were varied from 10 to 50 pmol/mL at 5 pmol/mL intervals with other parameters fixed ($K_d = 7.9$ pmol/mL), or K_d was varied from 3 to 15 at 2 pmol/mL intervals by changing k_{on} with other parameters fixed ($B_{max} = 25.7$ pmol/mL). For each TAC, B_{max} and K_d were estimated by the MI-GA from three points obtained by MI-SRTM for the single PET scan approach and they were estimated by the graphical analysis from three points obtained by the conventional SRTM for the three PET scan approach. Then, estimates were compared with the true values. In the single PET scan approach, B_{max} and K_d were also estimated without reference TAC by the MI-GA from three points of BP_{ND} and B obtained by the two-tissue compartment four-parameter model with the plasma input function shown in the Appendix.

Analysis of Monkey Studies

PET studies were performed on three cynomolgus macaques (weight 6.9 ± 2.1 kg) with the multiple-injection approach. One animal (monN) was a healthy monkey aged 5 years, and the others had a syndrome acquired Parkinsonism. Of these, one (monUP, aged 7 years) had hemiparkinsonism induced by injecting the selective neurotoxin, *N*-methyl-4-pheny1-1,2,3,6-tetrahydropyridine (MPTP) (0.4 mg/kg) into the right carotid artery (Bankiewicz *et al*, 1986), whereas the other (monBP, aged 5 years) had bilateral Parkinsonism induced by injecting MPTP (0.4 mg/kg) intravenously and intermittently (twice a week for a total of 14 injections) (Takagi *et al*, 2005). Each Parkinsonian animal showed typical Parkinsonian symptoms in the limbs (motor slowness, tremor) unilaterally or bilaterally. The PET scan was performed after the symptom reaching stable (6 months after the first injection of MPTP). Anesthesia was induced with ketamine (8.4 mg/kg, intramuscularly) and xylazine (1.7 mg/kg, intramuscularly) and maintained by intravenous propofol (6 mg/kg/h) and vecuronium (0.02 mg/kg/h) during the scan. The monkeys were maintained and handled in accordance with guidelines for animal research on Human Care and Use of Laboratory Animals (Rockville, National Institutes of Health/Office for Protection from Research Risks, 1996). The study protocol was approved by the Subcommittee for Laboratory Animal Welfare of the National Cardiovascular Center.

After the synthesis of [^{11}C]raclopride, nonradioactive raclopride was added so that targeted molar amount of raclopride would be administered for three injections (1.5, 10, and 30 nmol/kg); this was done by dividing the [^{11}C]raclopride diluted by nonradioactive raclopride into three portions with different volumes, containing the intended masses of raclopride. For the first injection, 1.9 ± 0.16 nmol/kg (57.0 ± 5.7 MBq) of [^{11}C]raclopride was administered by a bolus injection at the beginning of the scan. Fifty minutes later, the second [^{11}C]raclopride injection, 11.1 ± 0.56 nmol/kg (60.4 ± 8.8 MBq at the time of second injection) was administered by a bolus, and 50 mins after that, a bolus of 31.1 ± 2.1 nmol/kg (30.8 ± 4.4 MBq at the time of third injection) of [^{11}C]raclopride was administered again. Data were acquired for 150 mins (10 secs × 18, 30 secs × 6, 120 secs × 7, 300 secs × 6; total 50 mins for each injection). The specific radioactivity was 4.7 ± 2.2 GBq/μmol at the time of the first injection.

PET scans were performed using a PCA-2000A positron scanner (Toshiba Medical Systems Corporation, Otawara, Japan) that provides 47 planes and a 16.2 cm axial field-of-view. The transaxial and axial spatial resolution of the PET scanner were 6.3 and 4.7 mm full width at half maximum (Herzog *et al*, 2004). A transmission scan with a 3-rod source of ^{68}Ge-^{68}Ga was performed for 20 mins for attenuation correction before the administration of [^{11}C]raclopride. Radioactivity was measured in the three-dimensional mode and the data were reconstructed by a filtered back-projection using a Gaussian filter (3 mm of full width at half maximum). Region-of-interests (ROIs) were defined manually over the left and right striatum and cerebellum for PET images, and the radioactivity concentrations in these regions were obtained. For the left and right striatum, R_1, k_2, and BP_{ND} for each injection were estimated by the MI-SRTM. In addition, parametric images were generated, estimating each parameter voxel by voxel, using the MI-SRTM with a basis function method in which the model Equation (1) was solved using linear least squares for a set of basis functions, which enables the incorporation of parameter bounds (Gunn *et al*, 1997; Ikoma *et al*, 2009). B_{max} and K_d were estimated by the MI-GA from these BP_{ND} values of left and right striatum for three injections.

In the unilateral Parkinsonian animal, three PET scans with conventional single injection with different masses of [^{11}C]raclopride were also performed for comparison with results by the multiple-injection single PET scan approach. A PET scan with a bolus injection of 2.1 nmol/kg (50.6 MBq), 11.3 nmol/kg (60.4 MBq), or 31.1 nmol/kg (30.8 MBq) of [^{11}C]raclopride was obtained on separate days. PET data were acquired for 50 mins with the same protocol as the single PET scan approach. The values of R_1, k_2, and BP_{ND} were estimated by the SRTM, and B_{max} and K_d were estimated by the conventional graphical analysis.

Results

Simulation Study

Effect of Injected Mass on BP_{ND} Estimates: In the simulations, the value of BP_{ND}, estimated by the MI-SRTM, decreased as injected molar amount of raclopride increased, that is, concentration of bound raclopride became larger. The relationship between BP_{ND} and B^{ref} had a good linear correlation to some extent; however, it did not remain linear for large B^{ref} (Figure 2A). The regression line where $B^{ref} < 20$ pmol/mL was $BP_{ND} = -0.091B^{ref} + 2.4$, $R^2 = 0.997$ for the first injection. In the relationship between BP_{ND} and B^{ref}, BP_{ND} values of the third injection were higher than those of the first injection when B^{ref} was lower than 20 pmol/mL. The ratio B^{ref}/F^{ref} was almost the same as the BP_{ND} estimated by MI-SRTM, though it was a little smaller when B^{ref} was lower than 5 pmol/mL (Figure 2B).

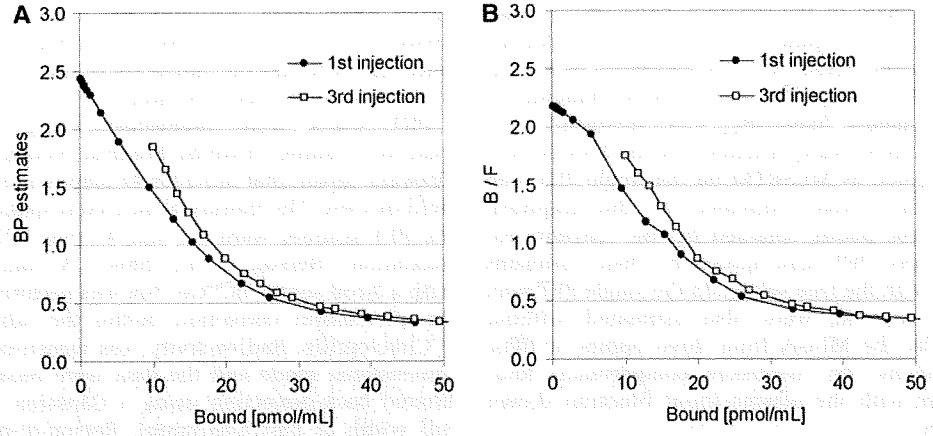

Figure 2 Relationship between specifically bound concentration and BP_{ND} (**A**) or B^{ref}/F^{ref} (**B**) estimates for the first and third injection in the simulations.

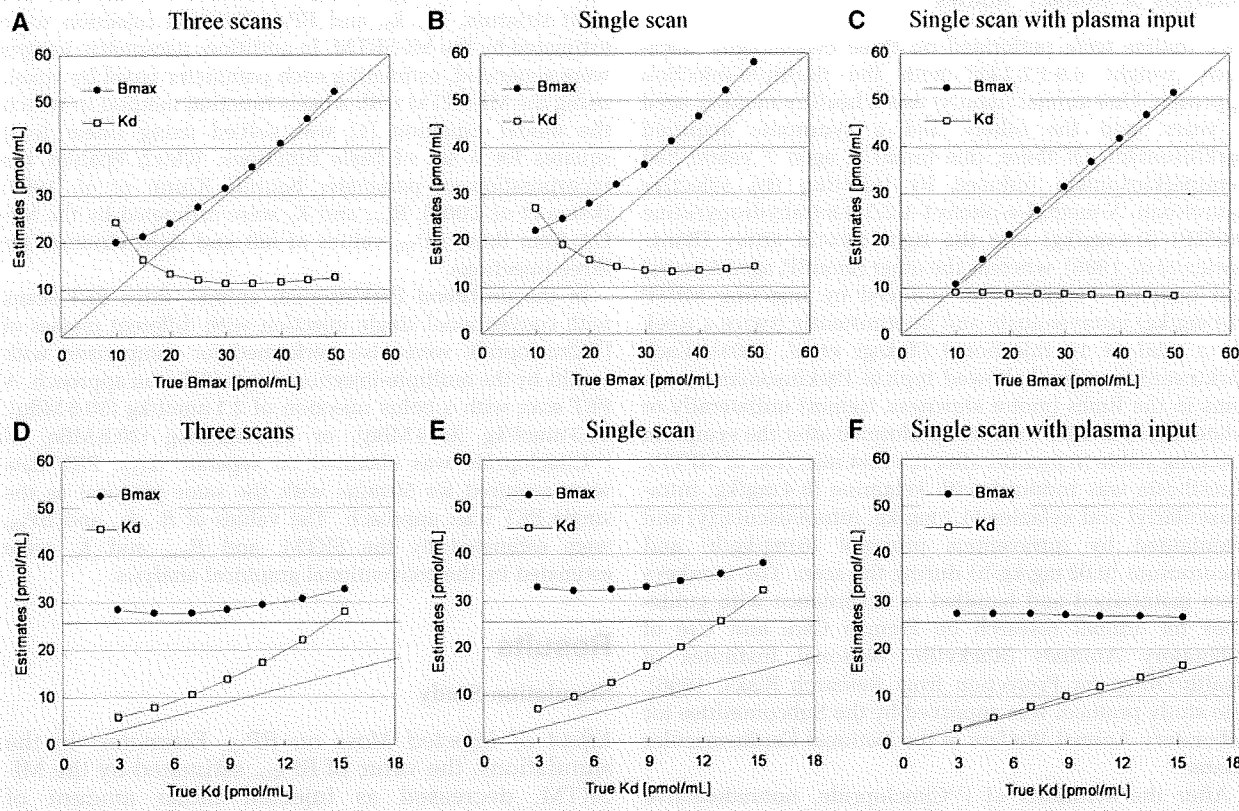

Figure 3 Relationships between estimates and true values of B_{max} and K_d for simulated TACs with various B_{max} and fixed K_d (**A**–**C**) and with various K_d and fixed B_{max} (**D**–**F**) by the three PET scan approach (**A**, **D**), multiple-injection single PET scan approach (**B**, **E**), and single PET scan approach with the plasma input function (**C**, **F**).

Estimation of B_{max} and K_d Values by the Multiple-Injection Graphical Analysis: The TACs were calculated for a range of possible B_{max} and K_d values, and the relationship between true and estimated B_{max} or K_d values was investigated for conventional three PET scan and the proposed single PET scan approaches. When B_{max} was varied, B_{max} and K_d were overestimated compared with the true values in both three PET scan and single PET scan approaches (Figures 3A and 3B). However, a good correlation was observed between true and estimated B_{max}, and there was little variation in estimated K_d when B_{max} was set higher than 20 pmol/mL. Similarly, when K_d was varied, although K_d and B_{max} were overestimated in both approaches, there was a good correlation between true and estimated K_d, and estimated B_{max} was constant (Figures 3D and 3E). In both cases, B_{max} and K_d estimates in the single

PET scan approach were higher than those in the three PET scan approach. In the TAC simulated with $B_{max} = 25.7$ and $K_d = 7.0$, estimated B_{max} and K_d were 27.8 and 10.5, respectively, in the three PET scan approach, and 32.3 and 12.6, respectively, in the single PET scan approach. In contrast to these approaches with the reference TAC, the overestimation of B_{max} and K_d was scarcely observed in the MI-GA with the plasma input function (Figures 3C and 3F).

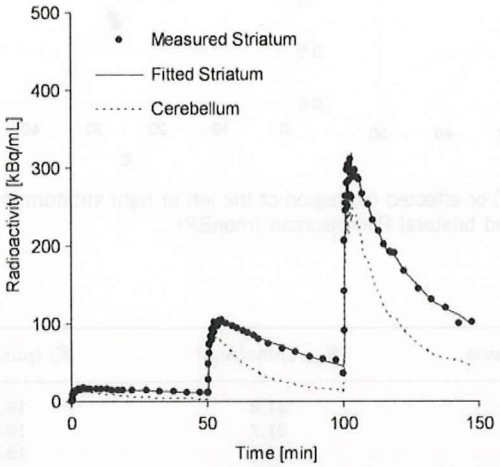

Figure 4 Measured TACs of the striatum and cerebellum and a fitted curve for the striatum using MI-SRTM in the monkey study by a single scan with sequential three injections of [^{11}C]raclopride.

Monkey Studies

Typical examples of TACs for the striatum and the cerebellum in the multiple-injection study are shown in Figure 4, and the parametric images of BP_{ND} for the first, second, and third injection, and images of B_{max} and K_d for the voxels in which BP_{ND1} was higher than 1.5 are shown in Figure 5. The estimated BP_{ND} decreased as the injected molar amount of [^{11}C]raclopride became larger in the second or third injection. Estimated BP_{ND1}, BP_{ND2}, and BP_{ND3} values were 2.3, 1.4, and 0.74, respectively, in the left striatum, and 2.6, 1.9, and 0.87, respectively, in the right striatum. The reduction in BP_{ND} was also observed in the parametric images.

The plots of MI-GA are shown in Figure 6. Plots of MI-GA for each of three animals were on the line, and B_{max} and K_d could be estimated as summarized in Table 1. Using the single scan approach for the hemiparkinsonian animal, B_{max} was 42.3 pmol/mL and K_d was 15.2 pmol/mL in the affected (right) striatum, and B_{max} was 32.3 pmol/mL and K_d was 13.0 pmol/mL in the contralateral (left) normal striatum. Corresponding estimates for the three scan approach were $B_{max} = 36.4$ and $K_d = 13.3$ pmol/mL in the right striatum and $B_{max} = 29.2$ and $K_d = 11.6$ pmol/mL in the

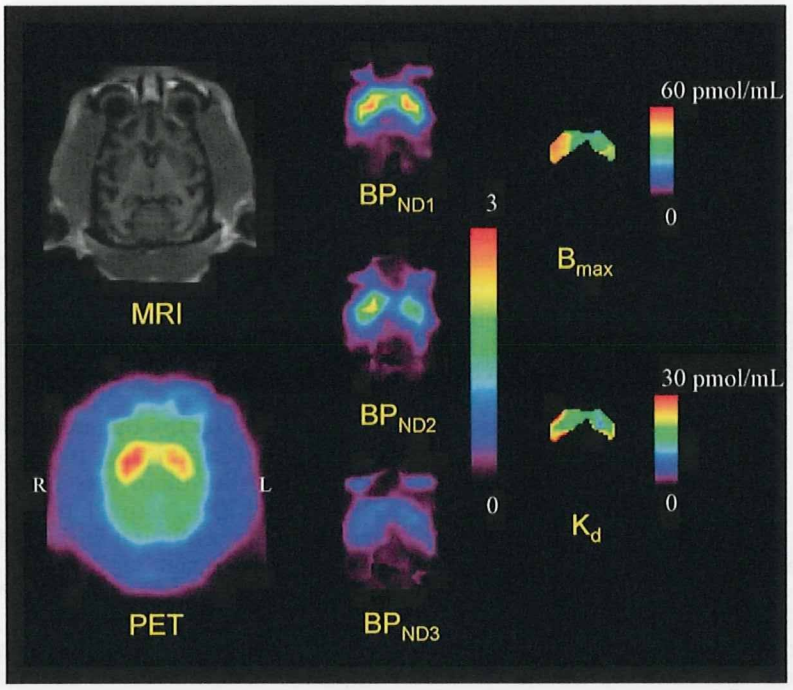

Figure 5 MRI and PET summation image (left) and parametric images of BP_{ND} for the first, second, and third injection (center) and parametric images of B_{max} and K_d for the voxels in which BP_{ND1} is higher than 1.5 (right) in the unilateral Parkinsonian (monUP) monkey study by a single scan with three sequential injections of [^{11}C]raclopride. Although ROI analysis disclosed higher B_{max} values in the MPTP-infused side of the striatum, the parametric image showed more evident increase of B_{max} in the dorsal and posterior parts of the striatum.

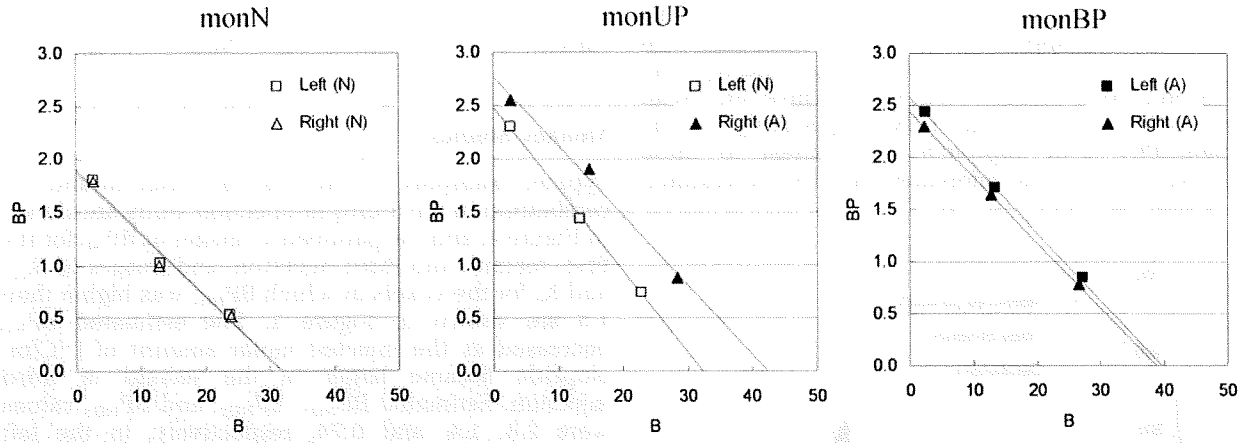

Figure 6 Single-scan, multiple-injection graphical analysis for normal (N) or affected (A) region of the left or right striatum in three monkeys that were normal (monN), unilateral Parkinsonian (monUP), and bilateral Parkinsonian (monBP).

Table 1 Estimated B_{max} and K_d values in three monkey studies

Scan protocol	*Subject*	*Region*	*Diagnosis*	B_{max} *(pmol/mL)*	K_d *(pmol/mL)*
Single scan	monN	L	N	31.8	16.7
		R	N	31.7	16.9
	monUP	L	N	32.3	13.0
		R	A	42.3	15.2
	monBP	L	A	39.6	15.4
		R	A	38.7	15.9
Three scans	monUP	L	N	29.2	11.6
		R	A	36.4	13.3

L, left striatum; R, right striatum; N, normal striatum; A, affected striatum.

left striatum. Both B_{max} and K_d of the single PET scan approach were slightly higher than those of the three PET scan approach. However, importantly, both approaches found that B_{max} in the affected striatum was higher than that in the normal striatum. The bilateral Parkinsonian animal showed B_{max} values of left = 39.6 pmol/mL, right = 38.7 pmol/mL, both of which were higher than those of the striatum of the normal animal or the normal striatum of the unilateral animal, but were very close to the affected striatum of the unilateral animal. The K_d values of the bilateral animal were not so different from other striatums.

Discussion

Density and Affinity Determination by Graphical Analysis with the Reference Region

In the graphical analysis for PET receptor studies, the values of B_{max} and K_d were estimated from the relationship between the ratio of bound to free concentrations and bound concentration at the time of transient equilibrium, using the TAC of the reference region (Farde *et al*, 1986). Some groups have used the value estimated from the distribution volume ratio − 1, instead of the B^{ref}/F^{ref} value of the y axis, because the values of B^{ref}/F^{ref} could change considerably with small changes in the time point of the transient equilibrium T_{eq} determined as the maximum C_b^{ref} (Logan *et al*, 1997; Doudet and Holden, 2003; Doudet *et al*, 2003). Distribution volume ratio or BP_{ND} is estimated from the kinetic analysis with TACs of target and reference regions, so it is not affected by the error of estimated T_{eq}. On the other hand, the value of $k'_3(t)$ in Equation (2) varies according to the concentration of bound raclopride, and estimates of BP_{ND} are considered to be an averaged value of specific binding over time, which is influenced by the dynamics of the free and bound raclopride. Despite this, in our simulation study of [^{11}C]raclopride, there was little difference between B^{ref}/F^{ref} and BP_{ND} estimated by the SRTM, and both had a linear correlation with B^{ref} (Figure 2). However, B^{ref}/F^{ref} became smaller than BP_{ND} and deviated from the linear relationship between B^{ref}/F^{ref} and B^{ref} in the region with low B^{ref} (Figure 2), especially for the TACs with high B_{max}. This may be a result of imperfect attainment of the transient equilibrium within the 50 mins scan duration for the TAC with high binding. There was little effect of the error of B^{ref} for the graphical analysis, in which B^{ref} varied widely among three injections, whereas the error of B^{ref}/F^{ref}

because of nonachievement of transient equilibrium had much effect on the graphical analysis as compared with BP_{ND}. Therefore, we estimated B_{max} and K_d by the graphical analysis with the relationship between BP_{ND} and B^{ref}.

In the simulations with various injected masses of [^{11}C]raclopride, it was shown that the relationship between BP_{ND} and B^{ref} became linear to some extent. However, BP_{ND} deviated from the linear relationship and approached a nonzero value when B^{ref} became larger (Figure 2). Therefore, in the B_{max} and K_d estimation by the graphical analysis with the reference TAC, points must be plotted within the range of the linear relation. As the relationship between BP_{ND} and B estimated from C_b using the plasma input function, without the reference TAC, remained linear even when B became large and the estimated BP_{ND} approached 0 (data not shown), this apparent saturation seemed to be owing to the reference region. Strictly speaking, the time course of free radioligand C_f is different from that of the reference region C_r (Figure 1) and C_f changes according to the specific binding that was affected by k_{on}, B_{max}, or administered mass of raclopride as pointed out by Ito *et al* (1998). Therefore, the time of the transient equilibrium estimated using C_b^{ref} was different from that estimated using C_b, and B^{ref} was often different as well. In addition, the value of BP_{ND} estimated by SRTM was lower than the BP_{ND} estimated from the two-tissue compartment model with the plasma input function.

This difference between the target and reference TAC affected the B_{max} and K_d estimates as well. In the simulated TACs with various B_{max} or K_d values, the B_{max} and K_d were overestimated compared with the true values even in the conventional three PET scan approach (Figure 3). On the other hand, the overestimation was not observed when B_{max} and K_d were estimated by the graphical analysis using C_f and C_b without the reference TAC (Figure 3), demonstrating that graphical analysis could determine B_{max} and K_d precisely if C_b were obtained correctly. However, the free and bound concentrations in the target region cannot be distinguished from the total concentration measured by PET scanning without arterial blood sampling, and in practical PET data, estimation of rate constants with the plasma input function is unstable and impractical. Therefore, in the usual graphical analysis, the TAC of reference region is used as the free radioligand concentration in the target region (Farde *et al*, 1989). The effect of the reference TAC on B_{max} and K_d estimates depends on the kinetics of the tracer in each region, which depends in turn on the particular tracers and species. In the simulated TACs of monkeys with [^{11}C]raclopride, there was a good correlation between true and estimated K_d or B_{max}, though estimates were biased. Therefore, we concluded the graphical analysis with reference TAC is practical for [^{11}C]raclopride studies, because it can detect the value of B_{max} or K_d in neurological or psychiatric disorders without arterial blood sampling.

Estimated Density and Affinity by the Multiple-Injection Approach

We applied the multiple-injection approach to the graphical analysis for B_{max} and K_d determination in an effort to shorten the total duration of the scanning protocol, and to obviate the need for several radiosyntheses for each animal. From the relationship between the BP_{ND} estimates and injected mass in the simulation study (Figure 2), the molar amounts of three injections were set as 1.5, 10, and 30 nmol/kg, so that the estimated BP_{ND} would be high, intermediate, and low within the range in which the linear correlation held. The injection interval was set to 50 mins, because it has been reported in monkey studies that 50 mins scan duration could provide reliable BP_{ND} estimates even for TACs with high and low BP_{ND} values (Ikoma *et al*, 2009). In our present studies on monkeys with this protocol, injected masses increased with each successive injection, but amounts of administered radioactivity remained fairly constant, i.e., 57, 60, and 31 MBq. Therefore, the signal to noise ratio of image quality did not change seriously for each injection.

In the usual graphical analysis by nonsequential multiple PET scans, the molar amount of administered [^{11}C]raclopride for each scan is adjusted by varying the specific activity of administered [^{11}C]raclopride. Several investigators have attempted to perform multiple injections of ligands with PET studies to obtain receptor density and affinity by changing specific activity with a detailed model equation (Delforge *et al*, 1995; Millet *et al*, 1995; Morris *et al*, 1996; Muzic *et al*, 1996; Christian *et al*, 2004; Gallezot *et al*, 2008). Meanwhile, our approach requires only one synthesis of [^{11}C]raclopride, which is split to three with different mass of raclopride with same specific activity. By keeping the specific activity throughout scan, we can directly interpret PET counts in pmol/mL unit.

In the simulations of B_{max} and K_d estimation with this single PET scan approach, B_{max} and K_d were overestimated compared with the true values, just as seen in the three PET scan approach. Furthermore, estimates of both parameters were higher than those in the three PET scan approach. In the single PET scan approach, the error because of assumptions of the reference tissue approach could be more severe than for the three PET scan approach, because the residual radioactivities at the times of the second and third injections could propagate to error of B^{ref} or BP_{ND} estimates. This was shown to be the case in the simulation study, in which the relationship between the BP_{ND} and B^{ref} in the third injection was a little different from that in the first injection (Figure 2). Furthermore, our approach assumes that BP_{ND} is promptly altered by the next injection, but this is in fact not exactly the case. We showed the bias of the estimated BP_{ND} related to this assumption (Ikoma *et al*, 2009), and the estimated B_{max} and K_d in this paper consequently could be biased. However, in the

simulations, B_{max} and K_d estimated by the MI-GA changed according to the variation of the true values (Figure 3), demonstrating this approach could be applied to the quantitative evaluation of B_{max} and K_d from a single session of PET scanning.

Monkey Studies

In the simulations, we demonstrated that the MI-GA could detect density and affinity of dopamine D_2 receptors. Furthermore, we demonstrated the validity of the proposed method using actual data from monkeys. As a result, the three BP_{ND} data points calculated from the single PET scan with three sequential injections of different administration masses were almost on a straight line, and estimated values of B_{max} and K_d were very close to those previously obtained *in vitro* ($B_{max} = 25.7$ pmol/g) (Madras *et al*, 1988) or *in vivo* by the conventional method in monkeys ($B_{max} = 22$ pmol/mL, $K_d = 13.5$ nmol/L) (Doudet *et al*, 2003). The estimates by the single PET scan approach were slightly higher than those by the three PET scan approach, and this was consistent with the results from the current simulations.

Although we investigated only three monkeys in this study, the values of B_{max} in the partially denervated striata was higher than in normal striatum, whereas the apparent affinity was unaffected by the MPTP lesions. Likewise Rinne *et al* (1995) reported a 35% increase in the D_2 B_{max} in the putamen contralateral to the side of predominant motor symptoms, without any discernible effect on apparent affinity. In our monkey measurements, in the hemilesioned monkey, the B_{max} was elevated by 31% on the denervated side. In the animal with bilateral MPTP lesion, the B_{max} in both striata was higher than in the normal animal, or in the unlesioned side of the hemiparkinsonian animal, despite no significant changes in K_d values: the results were consistent with those of the previous report.

In addition to the results of ROI analysis, which disclosed bulk D_2 receptor characteristics in the whole striatum, parametric imaging of B_{max} and K_d (as shown in Figure 5) suggested a potential significance in regional estimation of D_2 receptor characteristics. Although ROI analysis disclosed higher B_{max} values in the MPTP-infused side of the striatum, the parametric imaging showed the increase of B_{max} was more evident in the dorsal and posterior parts of the striatum. A similar finding of preferential lesion in dorsal and posterior parts of the striatum has been reported based on neurochemical and pathological assessments of MPTP-lesioned monkeys (Oiwa *et al*, 2003). As the current parametric imaging may have significant artifacts, such as those arising from low signal-to-noise ratio, partial volume effects, small number of points, the situation should be improved through the use of a higher resolution PET scanner.

Potential Limitations of the Multiple-Injection Graphical Analysis

The multiple-injection approach is able to assess the B_{max} and K_d for receptor studies in a single PET scan with single radiosynthesis, and shortened study period as compared with a conventional approach. This approach might also be applicable to other PET ligands and receptor types, but with several caveats: First, it is necessary to evaluate whether the reference region can be used as the free TAC of the target region. The kinetics of the target and reference regions is affected by the value of each rate constant, i.e., K_1, k_2, B_{max}, and K_d, that differ between species and radioligands. The difference between C_{ref} and C_f often causes an error in B^{ref}, and the estimated B_{max} and K_d should be interpreted with caution when the reference region has considerably different kinetics. Second, the molar amounts of administered ligand need to be selected such that the resultant BP_{ND} will be within the range in which the linear relationship between BP_{ND} and B holds. In the case of regions with low BP_{ND}, and small extent of the necessary linear relationship, it may be difficult to determine B_{max} and K_d reliably. Third, the interval of three injections should be determined so that the free ligand TAC has a transient equilibrium within the scan duration of each injection, especially when the injected mass is small, i.e., BP_{ND} is high. The radioligand [^{11}C]raclopride dissociates rapidly from the receptors, allowing equilibration of binding to be established *in vivo* within the time span of PET experiments (Farde *et al*, 1989; Ito *et al*, 1998). However, those ligands with slow kinetics, such as [^{18}F]fallypride require a longer scan duration such that the present graphical analysis may not be suitable in all instances. Despite these limitations, by optimizing the administered mass and the time interval between three injections of [^{11}C]raclopride, we have shown that the multiple-injection approach can determine B_{max} and K_d values as effectively as an approach using three separate scans, but within a single scan time of 150 mins.

Moreover, the bias of B_{max} and K_d estimated by the single scan approach with two injections was not larger than that by the single scan approach with three injections in the simulations (data not shown), and points of the second and third injections in MI-GA were almost on the same line in the monkey studies (Figure 6). Therefore, there is a possibility of reducing scan time and exposure further using only two injections, though the effect of statistical noise on estimates should be considered.

Conclusion

We developed the method for estimating B_{max} and K_d values in a single session of PET scanning with multiple injections of [^{11}C]raclopride. Our simulations showed that the MI-GA could detect B_{max} and K_d values by using the optimal injection protocol. We

also demonstrated in monkey studies that B_{max} and K_d values estimated by our proposed approach were proper compared with previous monkey studies or our studies by the conventional method. The proposed method made it possible to determine the dopamine D_2 receptor density and affinity by a 150 mins PET scan with three injections of [^{11}C]raclopride at 50 mins intervals.

Acknowledgements

We thank Dr Jun Takahashi (Kyoto University) for providing us animals for this study. This research was supported by the Ministry of Education, Culture, Sports, Science and Technology of Japan (MEXT) grant-in-aid for Young Scientists (B) (No. 20790839), grant-in-aid for Scientific Research (C) (No. 09019855) (TH), Kobe Cluster I and II, and the Ministry of Health, Labour, and Welfare of Japan (MHLW) Health Science Research Grant, H17-025 (TH, HI). We are grateful to members of Department of Investigative Radiology, National Cardiovascular Center Research Institute, for their support of PET experiment and for helpful suggestions.

Conflict of interest

The authors declare no conflict of interest.

References

Bankiewicz KS, Oldfield EH, Chiueh CC, Doppman JL, Jacobowitz DM, Kopin IJ (1986) Hemiparkinsonism in monkeys after unilateral internal carotid artery infusion of 1-methyl-4-phenyl-1,2,3,6-tetrahydropyridine (MPTP). *Life Sci* 39:7–16

Christian BT, Narayanan T, Shi B, Morris ED, Mantil J, Mukherjee J (2004) Measuring the *in vivo* binding parameters of [^{18}F]-fallypride in monkeys using a PET multiple-injection protocol. *J Cereb Blood Flow Metab* 24:309–22

Cross AJ, Crow TJ, Owen F (1981) ^{3}H-Flupenthixol binding in post-mortem brains of schizophrenics: evidence for a selective increase in dopamine D2 receptors. *Psychopharmacology (Berl)* 74:122–4

Delforge J, Pappata S, Millet P, Samson Y, Bendriem B, Jobert A, Crouzel C, Syrota A (1995) Quantification of benzodiazepine receptors in human brain using PET, [^{11}C]flumazenil, and a single-experiment protocol. *J Cereb Blood Flow Metab* 15:284–300

Doudet DJ, Holden JE (2003) Sequential versus non-sequential measurement of density and affinity of dopamine D_2 receptors with [^{11}C]raclopride: Effect of methamphetamine. *J Cereb Blood Flow Metab* 23:1489–94

Doudet DJ, Jivan S, Holden JE (2003) *In vivo* measurement of receptor density and affinity: comparison of the routine sequential method with a nonsequential method in studies of dopamine D_2 receptors with [^{11}C]raclopride. *J Cereb Blood Flow Metab* 23:280–4

Farde L, Ehrin E, Eriksson L, Greitz T, Hall H, Hedström CG, Litton JE, Sedvall G (1985) Substituted benzamides as ligands for visualization of dopamine receptor binding in the human brain by positron emission tomography. *Proc Natl Acad Sci USA* 82:3863–7

Farde L, Eriksson L, Blomquist G, Halldin C (1989) Kinetic analysis of central [^{11}C]raclopride binding to D_2-dopamine receptors studied by PET — A comparison to equilibrium analysis. *J Cereb Blood Flow Metab* 9: 696–708

Farde L, Hall H, Ehrin E, Sedvall G (1986) Quantitative analysis of D_2 dopamine receptor binding in the living human brain by PET. *Science* 231:258–61

Farde L, Wiesel FA, Hall H, Halldin C, Stone-Elander S, Sedvall G (1987) No D_2 receptor increase in PET study of schizophrenia. *Arch Gen Psychiatry* 44:671–2

Farde L, Wiesel FA, Stone-Elander S, Halldin C, Nordström AL, Hall H, Sedvall G (1990) D_2 dopamine receptors in neuroleptic-naive schizophrenic patients. A positron emission tomography study with [^{11}C]raclopride. *Arch Gen Psychiatry* 47:213–9

Gallezot JD, Bottlaender MA, Delforge J, Valette H, Saba W, Dollé F, Coulon CM, Ottaviani MP, Hinnen F, Syrota A, Grégoire MC (2008) Quantification of cerebral nicotinic acetylcholine receptors by PET using 2-[^{18}F]fluoro-A-85380 and the multiinjection approach. *J Cereb Blood Flow Metab* 28:172–89

Gunn RN, Lammertsma AA, Hume SP, Cunningham VJ (1997) Parametric imaging of ligand-receptor binding in PET using a simplified reference region model. *Neuroimage* 6:279–87

Guttman M, Seeman P (1985) L-dopa reverses the elevated density of D_2 dopamine receptors in Parkinson's diseased striatum. *J Neural Transm* 64:93–103

Hall H, Köhler C, Gawell L, Farde L, Sedvall G (1988) Raclopride, a new selective ligand for the dopamine-D_2 receptors. *Prog Neuropsychopharmacol Biol Psychiatry* 12:559–68

Herzog H, Tellmann L, Hocke C, Pietrzyk U, Casey ME, Kuwert T (2004) NEMA NU2-2001 guided performance evaluation of four Siemens ECAT PET scanners. *IEEE Trans Nucl Science* 51:2662–9

Ikoma Y, Watabe H, Hayashi T, Miyake Y, Teramoto N, Minato K, Iida H (2009) Quantitative evaluation of changes in binding potential with a simplified reference tissue model and multiple injections of [^{11}C]raclopride. *Neuroimage* 47:1639–48

Ito H, Hietala J, Blomqvist G, Halldin C, Farde L (1998) Comparison of the transient equilibrium and continuous infusion method for quantitative PET analysis of [^{11}C]raclopride binding. *J Cereb Blood Flow Metab* 18:941–50

Joyce JN, Lexow N, Bird E, Winokur A (1988) Organization of dopamine D_1 and D_2 receptors in human striatum: receptor autoradiographic studies in Huntington's disease and schizophrenia. *Synapse* 2:546–57

Köhler C, Hall H, Ogren SO, Gawell L (1985) Specific *in vitro* and *in vivo* binding of ^{3}H-raclopride. A potent substituted benzamide drug with high affinity for dopamine D-2 receptors in the rat brain. *Biochem Pharmacol* 34:2251–9

Lammertsma AA, Hume SP (1996) Simplified reference tissue model for PET receptor studies. *Neuroimage* 4:153–8

Logan J, Fowler JS, Volkow ND, Wang GJ, Ding YS, Alexoff DL (1996) Distribution volume ratios without blood sampling from graphical analysis of PET data. *J Cereb Blood Flow Metab* 16:834–40

Logan J, Volkow ND, Fowler JS, Wang GJ, Fischman MW, Foltin RW, Abumard NN, Vitkun S, Gatley SJ, Pappas N, Hitzemann R, Shea CE (1997) Concentration and occupancy of dopamine transporters in cocaine abusers with [^{11}C]cocaine and PET. *Synapse* 27:347–56

Madras BK, Fahey MA, Canfield DR, Spealman RD (1988) D1 and D2 dopamine receptors in caudate-putamen of nonhuman primates (*macaca fascicularis*). *J Neurochem* 51:934–43

Millet P, Delforge J, Mauguiere F, Pappata S, Cinotti L, Frouin V, Samson Y, Bendriem B, Syrota A (1995) Parameter and index images of benzodiazepine receptor concentration in the brain. *J Nucl Med* 36:1462–71

Mintun MA, Raichle ME, Kilbourn MR, Wooten GF, Welch MJ (1984) A Quantitative model for the *in vivo* assessment of drug binding sites with positron emission tomography. *Ann Neurol* 15:217–27

Morris ED, Babich JW, Alpert NM, Bonab AA, Livni E, Weise S, Hsu H, Christian BT, Madras BK, Fischman AJ (1996) Quantification of dopamine transporter density in monkeys by dynamic PET imaging of multiple injections of ^{11}C-CFT. *Synapse* 24:262–72

Muzic RR, Nelson AD, Saidel GM, Miraldi F (1996) Optimal experiment design for PET quantification of receptor concentration. *IEEE Trans Med Imaging* 15:2–12

Oiwa Y, Eberling JL, Nagy D, Pivirotto P, Emborg ME, Bankiewicz KS (2003) Overlesioned hemiparkinsonian non human primate model: correlation between clinical, neurochemical and histochemical changes. *Front Biosci* 8:155–66

Rinne JO, Laihinen A, Ruottinen H, Ruotsalainen U, Någren K, Lehikoinen P, Oikonen V, Rinne UK (1995) Increased density of dopamine D_2 receptors in the putamen, but not in the caudate nucleus in early Parkinson's disease: a PET study with [^{11}C]raclopride. *J Neurol Sci* 132:156–61

Scatchard G (1949) The attractions of proteins for small molecules and ions. *Ann NY Acad Sci* 51:660–72

Seeman P, Bzowej NH, Guan HC, Bergeron C, Reynolds GP, Bird ED, Riederer P, Jellinger K, Tourtellotte WW (1987) Human brain D_1 and D_2 dopamine receptors in schizophrenia, Alzheimer's, Parkinson's, and Huntington's diseases. *Neuropsychopharmacology* 1:5–15

Takagi Y, Takahashi J, Saiki H, Morizane A, Hayashi T, Kishi Y, Fukuda H, Okamoto Y, Koyanagi M, Ideguchi M, Hayashi H, Imazato T, Kawasaki H, Suemori H, Omachi S, Iida H, Itoh N, Nakatsuji N, Sasai Y, Hashimoto N (2005) Dopaminergic neurons generated from monkey embryonic stem cells function in a Parkinson primate model. *J Clin Invest* 115:102–9

Watabe H, Ohta Y, Teramoto N, Miyake Y, Kurokawa M, Yamamoto A, Ose Y, Hayashi T, Iida H (2006) A novel reference tissue approach for multiple injections of [C-11]Raclopride. *Neuroimage* 31:T73

Wong DF, Wagner Jr HN, Tune LE, Dannals RF, Pearlson GD, Links JM, Tamminga CA, Broussolle EP, Ravert HT, Wilson AA, Toung JK, Malat J, Williams JA, O'Tuama LA, Snyder SH, Kuhar MJ, Gjedde A (1986) Positron emission tomography reveals elevated D_2 dopamine receptors in drug-naive schizophrenics. *Science* 234:1558–63

Appendix

The multiple-injection two-tissue four-parameter compartment model is based on the following differential equations:

$$\frac{dC_f}{dt} = K_1 C_p(t) - (k_2 + k_3) C_f(t) + k_4 C_b(t) \qquad \text{(A1)}$$

$$\frac{dC_b}{dt} = k_3 C_f(t) - k_4 C_b(t) \qquad \text{(A2)}$$

where C_p is the radioactivity concentration of metabolite-corrected plasma, C_f and C_b are the concentrations of radioactivity for free and specifically bound ligand in tissue, respectively.

Equations (A1) and (A2) are solved with the radioactivity concentration of C_f and C_b at the time of injection, that is $C_f(0)$ and $C_b(0)$, then $C_f(t)$, $C_b(t)$ and total radioactivity concentration in tissue $C_t(t)$ are expressed as following equations:

$$\begin{aligned} C_f(t) = {} & \frac{K_1}{\alpha_2 - \alpha_1}\{(k_4 - \alpha_1)e^{-\alpha_1 t} - (k_4 - \alpha_2)e^{-\alpha_2 t}\} \otimes C_p(t) \\ & + \frac{1}{\alpha_2 - \alpha_1}\{(k_4 - \alpha_1)C_f(0) + k_4 C_b(0)\}e^{-\alpha_1 t} \\ & - \frac{1}{\alpha_2 - \alpha_1}\{(k_4 - \alpha_2)C_f(0) + k_4 C_b(0)\}e^{-\alpha_2 t} \end{aligned} \qquad \text{(A3)}$$

$$\begin{aligned} C_b(t) = {} & \frac{K_1 k_3}{\alpha_2 - \alpha_1}\left(e^{-\alpha_1 t} - e^{-\alpha_2 t}\right) \\ & \otimes C_p(t) + \frac{k_3}{\alpha_2 - \alpha_1}\left(C_f(0) + \frac{k_4}{k_4 - \alpha_1} C_b(0)\right)e^{-\alpha_1 t} \\ & - \frac{k_3}{\alpha_2 - \alpha_1}\left(C_f(0) + \frac{k_4}{k_4 - \alpha_2} C_b(0)\right)e^{-\alpha_2 t} \\ & + \left(\frac{k_3 k_4}{(k_4 - \alpha_1)(k_4 - \alpha_2)} + 1\right) C_b(0) e^{-k_4 t} \end{aligned} \qquad \text{(A4)}$$

$$\begin{aligned} C_t(t) = {} & \frac{K_1}{\alpha_2 - \alpha_1}\{(k_3 + k_4 - \alpha_1)e^{-\alpha_1 t} - (k_3 + k_4 - \alpha_2)e^{-\alpha_2 t}\} \\ & \otimes C_p(t) + \frac{k_3 + k_4 - \alpha_1}{\alpha_2 - \alpha_1}\left(C_f(0) + \frac{k_4}{k_4 - \alpha_1} C_b(0)\right)e^{-\alpha_1 t} \\ & - \frac{k_3 + k_4 - \alpha_2}{\alpha_2 - \alpha_1}\left(C_f(0) + \frac{k_4}{k_4 - \alpha_2} C_b(0)\right)e^{-\alpha_2 t} \\ & + \left(\frac{k_3 k_4}{(k_4 - \alpha_1)(k_4 - \alpha_2)} + 1\right) C_b(0) e^{-k_4 t} \\ \alpha_{1,2} = {} & \frac{(k_2 + k_3 + k_4) \mp \sqrt{(k_2 + k_3 + k_4)^2 - 4k_2 k_4}}{2} \end{aligned} \qquad \text{(A5)}$$

TISSUE ENGINEERING
Volume 13, Number 2, 2007

DOI: 10.1089/ten.2006.0185

A Reverse Transfection Technology to Genetically Engineer Adult Stem Cells

ARIMICHI OKAZAKI, M.Eng., JUN-ICHIRO JO, M.Eng., and YASUHIKO TABATA, Ph.D., D.Med.Sci., D.Pharm.

ABSTRACT

A new non-viral method of gene transfection was designed to enhance the level of gene expression for rat mesenchymal stem cells (MSCs). Pullulan was cationized using chemical introduction of spermine to prepare cationized pullulan of non-viral carrier (spermine-pullulan). The spermine-pullulan was complexed with a plasmid deoxyribonucleic acid (DNA) of luciferase and coated on the surface of culture substrate together with Pronectin of artificial cell adhesion protein. MSCs were cultured and transfected on the complex-coated substrate (reverse transfection), and the level and duration of gene expression were compared with those of MSCs transfected by culturing in the medium containing the plasmid DNA-spermine-pullulan complex (conventional method). The reverse transfection method enhanced and prolonged gene expression significantly more than did the conventional method. The reverse method permitted the transfection culture of MSCs in the presence of serum, in contrast to the conventional method, which gave cells a good culture condition to lower cytotoxicity. The reverse transfection was carried out for a non-woven fabric of polyethylene terephthalate (PET) coated with the complex and Pronectin using agitation and stirring culture methods. The two methods enhanced the level and duration of gene expression for MSCs significantly more than did the static method. It is possible that medium circulation improves the culture conditions of cells in terms of oxygen and nutrition supply and waste excretion, resulting in enhanced gene expression.

INTRODUCTION

THE RECENT ADVENT OF GENOME SCIENCES has elucidated genetic sequences that are related to disease occurrence and the proliferation and differentiation of cells for tissue repair. In addition, with the rapid development of cell biology and medicine regarding tissue regeneration, it has been possible to make use of various precursor and stem cells with high potential for proliferation and differentiation for cell therapy. However, because the cells are often not powerful therapeutically, it is of prime importance for successful cell therapy that a method of genetic cell engineering aiming at efficient activation and manipulation of cellular functions be developed. To achieve this genetic engineering of cells, virus carriers have mostly been used because of the high efficiency of gene transfection.[1–7] However, there are several problems to be resolved for clinical applications, such as the antigenicity and toxicity of the virus itself or the possibility of disease transfection. Therefore, efficient technology and methodology of gene transfection without virus vectors are expected.

Several research trials using non-viral gene carriers of cationized polymers and liposomes have been performed but do not always achieve the expected results in terms of transfection efficiency.[8–11] The level of gene expression is not as high as that of viral carriers, and the expression time period is generally short. As the conventional procedure of gene transfection, the non-viral carrier is complexed with a plasmid deoxyribonucleic acid (DNA) and then added to the cell culture medium for transfection. In this case, serum

Department of Biomaterials, Field of Tissue Engineering, Institute for Frontier Medical Sciences, Kyoto University, Kyoto, Japan.